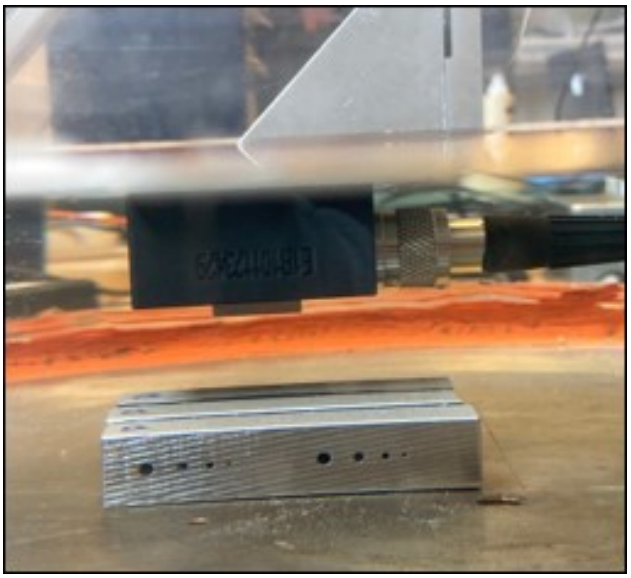

Ultrasonic Signal Response from Internal Manufactured Defects in Laser-Based Powder Bed Fusion (PBF-LB) Manufactured superalloys.

Master's thesis in Materials Engineering

ANUPAMA SURENDRAN

DEPARTMENT OF INDUSTRIAL AND MATERIALS SCIENCE

CHALMERS UNIVERSITY OF TECHNOLOGY
Gothenburg, Sweden 2026
www.chalmers.se

Master's thesis 2026

Ultrasonic Signal Response from Internal Manufactured Defects in Laser-Based Powder Bed Fusion (PBF-LB) Manufactured superalloys.

ANUPAMA SURENDRAN

CHALMERS
UNIVERSITY OF TECHNOLOGY

Department of Industrial and Materials Science
Division of Materials and Manufacture
Chalmers University of Technology
Gothenburg, Sweden 2026

Ultrasonic Signal Response from Internal Manufactured Defects in Laser-Based Powder Bed Fusion (PBF-LB) Manufactured superalloys.

ANUAPAM SURENDRAN

Supervisor: Mattias Broddegaard,Siemens Energy AB,
Håkan Wirdelius , Department of Engineering Science ,University West ,
Mikael Sahl,Department of Engineering Science,University West
Examiner: Mats Norell,Department of Industrial and Materials Science

Master's Thesis 2026
Department of Industrial and Materials Science

Chalmers University of Technology
SE-412 96 Gothenburg
Telephone +46 31 772 1000

Cover: Conventional Ultrasonic Testing of Inconel 939 Block 1 Using 1.5" Probe at 18 mm Water Path.

Typeset in LaTeX
Printed by Chalmers Reproservice
Gothenburg, Sweden 2026

Ultrasonic Signal Response from Internal Manufactured Defects in Laser-Based Powder Bed Fusion (PBF-LB) Manufactured superalloys.
ANUPAMA SURENDRAN
Department of Industrial and Materials Science.
Chalmers University of Technology

Abstract

Additive manufacturing (AM) is an advanced technology reshaping global product fabrication by enabling lightweight and complex structures directly from CAD models [1]. While AM provides design freedom and material efficiency, challenges remain in ensuring consistent quality, as defects such as porosity, microcracks, and lack of fusion (LOF) voids can degrade mechanical performance [7–9]. Non-destructive testing (NDT) methods are therefore critical, with X-ray Computed Tomography (XCT) and Ultrasonic Testing (UT) emerging as the most promising despite limitations of cost, speed, and geometry sensitivity [16,20]. UT, in particular, enables early detection of internal flaws without damaging the component, and recent advances such as phased array and laser-based techniques are expected to further enhance inspection capability [2,24,25].

This study evaluates the ultrasonic signal response from intentionally introduced defects in PBF-LB manufactured Alloy 247 and Inconel 939 samples. Both immersion UT and PAUT were applied to investigate the influence of defect morphology, orientation, and surface finish. Results showed that defects down to 0.4 mm could be reliably detected when oriented perpendicular to the scanning surface. Machined surfaces significantly improved defect detectability, while partially melted powder around defects increased scattering and reduced signal clarity. Among probes, the 3.25" transducer provided the most consistent response due to its larger aperture, which enhanced beam focus, signal strength, and defect detectability across varied geometries and surface conditions. Defect morphology strongly influenced detectability, with angled and roof-shaped defects showing reduced visibility compared to cylindrical or spherical ones.

Comparison of inspection methods demonstrated that PAUT enhanced sensitivity and imaging in geometrically complex regions, whereas XCT provided more accurate defect characterization but with slower scan speed and higher cost. These findings highlight the importance of probe selection, surface condition, and defect morphology for developing robust in-situ inspection strategies and support the integration of PAUT and XCT as complementary methods for standardized quality control in metal additive manufacturing.

Keywords:Additive Manufacturing,PBF-LB, Ultrasonic Testing,XCT ,Phased Array Ultrasonic Testing,Internal Defects.

Acknowledgements

I would like to express my sincere gratitude to Dr. Mats Norell, my mentor at Chalmers University, for his invaluable guidance, encouragement, and for instilling in me a commitment to excellence and ambition.

I am deeply appreciative of the unwavering support provided by my supervisor, Mattias Broddegaard at Siemens Energy AB, as well as Prof. Håkan Wirdelius and Mikael Sahl at University West. Their insightful feedback and expertise have been instrumental in shaping this thesis.

My heartfelt thanks extend to Hanna Sivervik and Siemens Energy AB for generously funding this research. I am also grateful to the Materials Department at Siemens Energy AB for providing access to the essential equipment and laboratory facilities necessary for conducting this study.

I sincerely thank Dr. Erik Lindgren at University West and Produktionstekniskt Centrum (PTC) for granting me the opportunity to utilize XCT and PAUT techniques. I also appreciate my colleagues in the Materials Department at Siemens Energy AB and my fellow students in the Materials Engineering program for their collaboration and for making this academic journey an enriching experience. Additionally, I am thankful to my colleagues in the Department of Industrial and Materials Science for their support and encouragement.

Finally, I express my deepest gratitude to my parents, family, and friends for their unwavering belief in me and their constant encouragement throughout this endeavor. Their support has been invaluable.

Anupama Surendran, Gothenburg,

March 2026

List of Acronyms

Below is the list of acronyms that have been used throughout this thesis listed in alphabetical order:

ACS	Arm Control System
AM	Additive Manufacturing
CAD	Computer Aided Design
CT	Computed Tomography
EDM	Electrical Discharge Machining
ET	Eddy Testing
FBH	Flat Bottom Holes
FMC	Full Matrix Capture
FPX	Focus PX
IS	Internal Spheres
LOF	Lack of Fusion Voids
MAM	Metal Additive Manufacturing
MP	Material Path
NDE	Non-Destructive Examination
NDT	Non-destructive Testing
PA	Phased Array
PAUT	Phased Array Ultrasonic Testing
PBF-LB	Powder Bed Fusion-Laser Beam
SEM	Scanning Electron Microscope
S/N	Signal -to-Noise Ratio
TFM	Total Focusing Method
TOF	Time of Flight
TR	Transmitter - Receiver Probe
UT	Ultrasonic Testing
VT	Visual Testing
WP	Water Path
XCT	X-ray Computed Tomography

Nomenclature

Below is the nomenclature of indices, sets, parameters, and variables that have been used throughout this thesis.

Parameters

f	frequency of the sound wave
T	Time period
λ	Wavelength of the ultrasonic wave
c	velocity of sound in a medium
Z	Acoustic Impedance
ρ	Material Density
V	Sound Velocity
D	Diameter of the Piezoelectric Transducer
L	Length of the sample block
W	Width of the sample block
H	Height of the sample block
N	Near field distance
θ_i	Angle of Incidence Sound Wave
θ_1	Angle of Reflected Longitudinal Sound Wave
θ_2	Angle of Refracted Longitudinal Sound Wave
θ_3	Angle of Reflected Shear Sound Wave
θ_4	Angle of Refracted Shear Sound Wave
V_i	Velocity of Incidence Sound Wave
V_{L1}	Velocity of Reflected Longitudinal Sound Wave
V_{L2}	Velocity of Refracted Longitudinal Sound Wave
V_{L3}	Velocity of Reflected Shear Sound Wave
V_{L4}	Velocity of Refracted Shear Sound Wave

X, Y, Z	Linear Axis
L	External Axis
C	Rotational Axis
F	focal length of Probe in water
C_{tm}	Sound Velocity in test specimen
C_w	Sound Velocity in water
R_a	Surface Roughness

Contents

List of Figures

List of Tables

1
Introduction

1.1 Siemens Energy

Siemens is a global pioneer in the field of electrical engineering which began as a startup firm in 1847. Siemens has played a significant role in shaping technological advancement not only in Germany but also across Europe and the rest of the world. In 1847, Werner von Siemens laid the foundation for the Siemens AG in Berlin, which built Europe's first long-distance telegraph line. In 1866, Werner von Siemens laid a foundation for the new age of electricity. He recognized the immense potential of the dynamo-electric principle and believed that the value of invention lies in its practical applications. He successfully transformed mechanical energy into electrical energy without the application of permanent magnets, making it applicable to daily life [3]. As an independent firm, Siemens has started a new chapter in the history of energy technology.

In 1897, Siemens built its first electrical power plant in South Africa [4]. In 1997, Siemens opted to acquire the fossil fuel power plant company of US company Westinghouse. In 2004, they bought Bonus Energy, a leading company in offshore wind turbine. In 2020, a new independent company Siemens Energy was founded, which is a subsidiary of Siemens. Siemens Energy is a well-known company across the energy value chain, along with a comprehensive portfolio for power utilities, power generators, the oil and gas industry, transmission grid operators, and other energy-intensive sectors, with 90,000 employees all over the world. Siemens Energy in Finspång has brought a revolutionary transformation in the development, manufacturing, and maintenance of gas turbine components. By utilizing the 3D printing process, complex metal parts can now be produced, opening a wide design possibility in a faster and more flexible manner as compared to conventional technology [5].

1.2 Background

Additive manufacturing (AM) is a revolutionary technology that transforms product fabrication and material production on a global level. This is mainly due to its fabrication flexibility to print structures having unique micro-structure and radial geometries.

AM is a flexible and customized manufacturing technique capable of fabri-

cating near-net-shaped 3-dimensional parts from a CAD model through the layer-by-layer deposition of metal powder guided by a computer. The AM components have excellent mechanical properties as compared to conventional casting. Metal additive manufacturing (MAM) is commonly used in automotive industries, aircraft assembly, and power tool industries which offers a wide range of advantages the production of lightweight components having geometric complexity and customized designs at high quality, minimal internal defects, minimal material wastage, and low cost[6]. For the fabrication of AM alloys parts, the Powder Bed Fusion-Laser Beam (PBF-LB) technique is commonly used, where the laser beam is used to fuse the metal powder to print the predetermined design.

One of the challenges faced by Additive manufacturing is quality control depending on the process parameters and the energy used for fusing the material offering unique microstructure and flaws or defects in the final product. Inter-layers and intralayer defects can be detected in PBF- LB components when examined using SEM and microcomputed tomography [7]. The most found defects in AM components are gas porosity, microcracking, and lack of fusion voids (LOF) [8]. Among these defects, porosity stands as a vital concern due to its potential impact on the strength of the components. LOF is mainly due to the improper bonding between the layers before the material is completely fused which affects the fatigue and tensile strength of the AM parts or components [9]. The presence of ample-size voids acts as a stress concentrator which leads to crack initiation sites and reduces the load-carrying capacity of the components. Various NDT techniques are employed to effectively identify different types of defects in AM components.

The introduction of artificial defects is a common method for ensuring material quality, following Nondestructive testing (NDT) guidelines, and measuring the mechanical properties for performance and safety standards [10]. The seeded process must accurately replicate the natural defects that occur during actual printing processes. The optimal defects can be created by systematically adjusting process parameters rather than introducing artificial flaws through methods like drilled holes or electrical discharge machining (EDM). This approach ensures that the defects accurately reflect real manufacturing conditions. The challenges with artificial defects like flat bottom or side drilled holes are that their size, morphology, and distribution do not accurately represent the naturally occurring defects [11-12].

The inspection of AM-produced parts is indeed a significant challenge that poses limitations on the widespread adoption of the Metal Additive Manufacturing (MAM) technique. To achieve this and for the widespread use of AM technology, quality assurance, and control are essential. Since AM is utilized for high-value applications where component failure cannot be allowed [13-15]. In most cases, the inspection of AM components has been assessed by destructive methods or X-ray computed tomography (XCT) [16]. Other NDT methods used in AM inspection are visual inspection testing (VT) [17], eddy current testing (ET) [18], ultrasonic testing (UT), etc. The application of most of the NDT techniques for the inspection in MAM faces some challenges due to complex geometry, deep defects, and

surface roughness [19]. The most promising methods among them are XCT and UT. However, the major limitation of XCT is that the scan resolution depends on the maximum achievable magnification and the dimension of the part, due to this XCT has a slow scan speed and high cost of inspection when compared to other inspection techniques [20].

Ultrasonic inspection is one of the most powerful NDT inspection techniques for identifying and examining cracks, subsurface, and internal defects. UT can detect flaws as deep as several meters in most metals and has good penetration power, whereas material thickness serves as one of the limiting factors for other NDT methods. In this method, high-frequency sound waves in the range of MHz are emitted into the test material under inspection and the sensitivity of UT in detecting the defects depends on the testing frequency. The emitted wave propagates due to sound attenuation and is reflected at the internal defects, boundaries, and joints. Due to the high sensitivity of the UT equipment and high penetration power of the sound wave, Ultrasonic Testing is commonly used as it is a low-cost inspection technique. Palanisamy et al [21] conducted an experiment to identify the effect of surface roughness on the ultrasonic signals on aluminium die casting samples. They concluded that it is difficult to detect the near-surface defect due to the clustered front wall echoes reflected from the rough surface and the most suitable probe used for the inspection of aluminium die caste is the one with a frequency range of 5 to 10 MHz. Simonetti et al [22,23] suggested the use of ice to encapsulate the AM parts, as the speed of the longitudinal wave in ice is 2.5 times more than in water. The experiment is conducted by freezing the water before the inspection, so ice can fill the internal cavities and ultrasonic waves are allowed to propagate through all parts. This technique is called cryo ultrasonic nondestructive evaluation (NDE), which helps to inspect complex AM parts. Heavy wall components with complicated geometries are now subjected to phased array ultrasonic testing (PAUT), a method that employs multi-element transducers that can transmit and receive ultrasonic signals independently at different intervals thereby reducing inspection times and increasing reliability and sensitivity [24,25].

The objective of this project is to,

• Examine how the Ultrasonic signal response from internal flaws is impacted by the melted and partially melted particles.

• Examine the impact of external surface structure (one sample is in as-printed form, while the other has a surface that has been machined) on how the ultrasonic signal reacts to printed imperfections.

• Study the variation of UT signal response from reference reflectors(standardized defects or targets used to calibrate and verify the sensitivity of ultrasonic inspection systems,here one of the printed defect is used as a reference reflector) using various probes and determine whether it is feasible to use printed imperfections as a reference reflector utilising the PBF-LB approach.

2

Theory

Ultrasonic testing uses mechanical waves generated by time-varying deformation or the vibration of atoms within a medium like solid, liquid, or gas. These waves travel through the medium at a specific speed or velocity, in an expectable direction, and when they strike the interface having a different medium at an oblique angle, the wave gets reflected or refracted. UT uses high-frequency sound waves, in the range of 0.5 MHz to 20 MHz, for inspection. These high-frequency waves are generated by a piezoelectric transducer, which can convert the electrical signals to mechanical vibrations and vice versa. The emitted wave propagates through the material with some energy loss (attenuation) due to the material characterization. And when the sound waves strike the interface, defects, or joints, it gets scattered and some of the sound waves are reflected back to the transducer. The reflected sound wave is detected and analyzed to identify the presence and location of internal flaws. The degree of reflection depends on the roughness of the material, and the physical state of the interface i.e, most of the sound wave will be reflected at metal–gas interface and partially reflected at metal–liquid and metal–solid interface [26]. The output signal from the transducer can be displayed in several formats. The most used formats are A-scan, B-scan, and C-scan presentation. A-scan represents pulse amplitude verse elapsed time (Time of Flight, TOF) i.e, the amplitude of reflected signal along the Y-axis and the elapsed time or flaw/ discontinuity depth on the X-axis. B-scan represents the cross-sectional view of the test specimen so that the length of the defect and its depth from the surface can be identified. And C–scan represents the plan view of a test sample where the external details of the test specimen were projected.

2.1 Characteristics of Wave Propagation

• Frequency (f) and Time period (T).

Ultrasonic vibrations travel in the form of a wave similar to the light wave. But ultrasound requires medium to propagate, like solid, liquid or gas. Frequency (f) of the sound wave is same as that of the oscillation of atoms in a medium (i.e, number of cycles per second). And is usually measured in Hertz (Hz)

$$f = \frac{1}{T} \tag{2.1}$$

The time taken to complete one cycle is known as the time period (T), measured in seconds.

• Wavelength (λ).

During one oscillation, the wave travels a certain distance in the medium. This distance is referred to as wavelength (λ).

$$\lambda = \frac{c}{f} \tag{2.2}$$

Where, c is the velocity of sound in a medium.

• Acoustic impedance (Z).

Acoustic impedance (Z) is the resistance offered by a material to the propagation of sound waves. It is determined by the product of material density ρ and the sound velocity V.

$$Z = \rho * V \tag{2.3}$$

• Sensitivity and Resolution.

Sensitivity is the ability of an ultrasonic transducer to detect echoes from small flaws. The greater the received signal from the flaw, the more sensitive the transducer.

Resolution is the ability of a transducer to produce simultaneous and distinct echoes from two flaws located nearly the same position with respect to ultrasound beam.

2.2 Mode of Propagation

In solids, sound can propagate in four modes of propagation which are defined by the oscillatory motion of the particles in the medium. Sound can propagate in longitudinal waves, shear/transverse waves, surface/Rayleigh waves, and plate/lamb waves in materials. In these, longitudinal waves and shear waves are commonly used modes of propagation for ultrasonic testing.

1. Longitudinal or Compression waves

   A longitudinal wave is characterized by the particle oscillating in the longitudinal direction or the direction of wave propagation. Audible sound waves propagate as longitudinal waves. Longitudinal waves travel the fastest among the different wave modes.

2. Transverse or Shear Waves

   Transverse or shear waves are defined by the particles oscillating in the direction perpendicular to the direction of wave propagation. Shear waves travel with a slow velocity and shorter wavelength than longitudinal waves of the same frequency. These types of waves are used for the angle beam testing in UT. Shear waves only exist in solid medium, not in liquid and gaseous medium. They can be mode converted to longitudinal waves by refraction or reflection at the boundaries.

3. Surface or Rayleigh Waves

   Surface or Rayleigh waves are defined by the elliptical particle motion. This oscillatory motion travels along the surface of the test specimen and penetrates to a depth of one wavelength.

4. Lamp or Plate Waves

   Lamp or plate waves are found only in thin plates, material thickness is about one wavelength, where the particle oscillates in a complex mode.

2.3 Mode Conversion and Snell's law

In most ultrasonic inspections, longitudinal and transverse waves are used for flaw detection. When these waves incident on the interface of the materials at an oblique angle, the waves undergo reflection, transmission, and mode conversion. Mode conversation of the wave is the change in the wave motion, which occurs when the wave strikes at the interface of two mediums having difference in acoustic impedance.

Sound waves at high frequencies are directional so the wave used for the ultrasonic inspection should be well defined. When a sound wave incident at an interface between materials, it can undergo reflection or refraction. Reflection occurs when the incident wave strikes the boundary at a perpendicular angle, causing it to bounce back. On the other hand, refraction takes place when the incident wave hits the boundary at an oblique angle, causing the wave to change direction. If the sound wave travels along a straight path parallel to the boundary, it will continue in the same straight direction. The behavior of the refracted or reflected wave can generally be determined using Snell's law. This law states that the ratio of the sine of the angle of incidence to the sine of the angle of refraction or reflection is equal to the corresponding velocities of the incident and refracted or reflected sound waves within the medium [27].

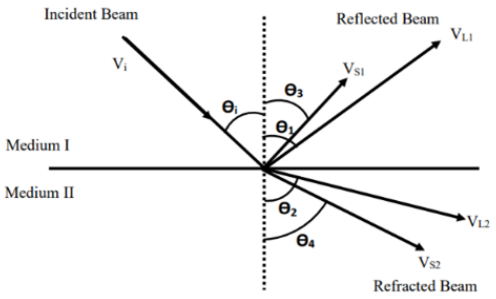

Figure 2.1: Snell's law representation

$$\frac{sin\theta_i}{V_i} = \frac{sin\theta_1}{V_{L1}} = \frac{sin\theta_2}{V_{L2}} = \frac{sin\theta_3}{V_{S1}} = \frac{sin\theta_4}{V_{S2}} \tag{2.4}$$

Where,
θ_i is the angle of the incident sound waves.
θ_1 and θ_2 are the angle of reflected and refracted longitudinal sound waves.
θ_3 and θ_4 are the angle of reflected and refracted shear sound waves.
V_i is the velocity of incident sound waves.
V_{L1} and V_{L2} are the velocity of reflected and refracted longitudinal sound waves.
V_{S1} and V_{S2} are velocity of reflected and refracted shear sound waves.

2.4 Sound Field

A piezoelectric transducer with a single element can be considered as a collection of point sources, each of which emits sound waves to the materials. These waves interfere with each other and result in fluctuation of wave intensities i.e, the echo will go through a series of maximum and minimum amplitude and finally ends in a maximum amplitude at a distance N from the transducer. This region is referred to as Near field. The region beyond the maximum amplitude is referred to as Far field, where there is only minor variation in wave intensity. All the inspection is performed at the far field as the defect or flaw inspected under near field is difficult to inspect using amplitude technique due to the variation in the amplitude and thus shows multiple indications. The length of the near field for a certain probe depends on the probe diameter and the wavelength of the ultrasonic signal in a particular medium. Near field distance (N) can be calculated by [27]

$$N = \frac{D^2}{4\ \lambda} = \frac{D^2 f}{4V} \tag{2.5}$$

Where, N is the Near field length.
D is the diameter of the piezoelectric transducer.
λ is the wavelength of the ultrasonic wave .
V is the sound velocity.
f is the frequency of the sound wave.

2.5 Transducer/Probe

Ultrasonic transducer, which is also known as probe, converts electrical voltage received from the UT pulser into sound wave and vice versa, using the piezoelectric effect. If the single crystal serves as both transmitter and receiver, then the probe is known as single crystal probe. On the other hand, if echo receiver is a separate crystal, then the probe is called transmitter-receiver probe (TR). There are different types of transducers, contact transducers, dual transducers, angle beam transducers, immersion transducers etc.

• Contact transducer:

These transducers have direct contact with the test specimen. The piezoelectric element is protected in a rugged casing to withstand sliding contact with different materials. A coupling medium is applied between the test sample and the transducer to ensure sound transmission.

• Dual transducer:

These transducers consist of two crystals which act as transmitter and receiver, housed in same case, separated by acoustic barrier.

• Angle beam transducer:

They use the principle of mode conversion and refraction to produce transverse or longitudinal waves in the test specimen by attaching a wedge to the transducer.

• Immersion transducers:

These are single element longitudinal wave transducers, with 1/4 wavelength acoustically matched to the water. They are used in the application where the test samples are fully or partially immersed in water.

2.6 Phased Array Ultrasonic Technology

The main characteristic of phased array ultrasonic testing is its ability of computer-controlled excitation (delay and amplitude) of individual elements in a multi-element probe. The excitation of this multi-element piezoelectric probe can generate a focused and steered beam by modifying the beam parameters like angle, focal distance, focal stop, time delay etc; to produce a beam in phase by means of constructive interference by changing the progressive time delay of active elements in the probe.

• Phased Array (PA)Probe

These probes are made of various small piezoelectric elements. Each of these small elements are pulsed individually by computer calculated timing and the response signal from each element are recorded separately. To achieve the desired focusing, each element in the phased array probe is fired at different time intervals. These delay times, known as focal laws, are calculated automatically by the inspection software. The focal laws play a crucial role in beam focusing during the inspection process.

Usually, PA probe have a frequency range between 1MHz to 17 MHz and have 10 to 128 elements. PA probes are made in a variety of sizes and shapes for different applications. In PA probe, elements are arranged in several different configurations like linear PA, annular PA, concave PA, convex PA etc. In a linear phased array probe, the piezoelectric elements are arranged in a straight line. However, in an annular phased array probe, the elements are arranged in circular rings with a

common center. On the other hand, in a convex phased array probe, the elements are arranged in an arched line.

Although annular array probes are not commonly used as linear array probes due to certain limitations, such as the no beam steering, they possess unique characteristics that make them superior for certain applications. Their unique geometry enables them to focus on significant depths within a material, achieving both symmetric and circular focal points.

3
UT Equipment

The ultrasonic testing conducted in this study comprises Immersion Testing and Phased Array Ultrasonic Testing (PAUT), two widely used Non-Destructive Testing (NDT) techniques for material inspection.

The Immersion Testing was performed at the NDT laboratory of Siemens Energy AB in Finspång, Sweden. This method involves submerging the test specimen in a water tank, where water acts as a couplant to facilitate the transmission of ultrasonic waves. It allows for highly accurate and repeatable measurements, making it ideal for detecting internal defects, evaluating material integrity, and characterizing structural components.

On the other hand, Phased Array Ultrasonic Testing (PAUT) was conducted at the NDT laboratory of University West in Trollhättan, Sweden. PAUT is an advanced ultrasonic technique that utilizes multiple elements within a probe to generate and steer sound beams electronically. This method enables a more flexible and comprehensive evaluation of complex geometries and discontinuities, providing higher resolution imaging compared to conventional ultrasonic testing.

3.1 Conventional Immersion Ultrasonic Testing

Immersion UT testing was performed at Siemens Energy laboratory, in accordance with EN ISO 16810 standards. Focus PX conventional immersion testing instrument is used for the inspection with 3 probes having different focal lengths. The specifications of the probes shown in Figure 3.1 are as follows:

- Harisonic iR1008 with 1.5-inch point focus in water (10 MHz, 0.5-inch diameter).
- Harisonic iR1008 with 2.5-inch point focus in water (10 MHz, 0.5-inch diameter).
- Panametrics V327 with 3.25-inch point focus in water (10 MHz, 0.375-inch diameter).

The Harisonic iR1008 with 1.5-inch and 2.5-inch probes are square-bodied probes, while the Panametrics V327 with a 3.25-inch point focus is a round-bodied probe. Both types of probes can scan surfaces parallel to the immersion floor tank. The transducer with a square housing is used to scan surfaces perpendicular to the

immersion tank, while the round-profile transducer can be replaced with a punch tool to mark the position where the probe is aimed. Each probe has a different focal length, which is the distance between the probe surface and the focus point on the material in the water.

(a) (b) (c)

Figure 3.1: Conventional immersion UT probes: (a) Probe with 1.5" point focus in water, (b) Probe with 2.5" point focus in water, (c) Probe with 3.25" point focus in water.

3.1.1 Focus PX (FPX)

The processor hardware Focus PX collects the transducer and encoder data and sends it to PC acquisition software via LAN cable. This unit can be connected to single crystal or twin crystal transducers where single crystal probe is connected to the P1/R1 port while the twin crystal probe is connected to P1 port. The inspection data is processed by Focus PC software. Prior to the initial recording, the FPX needs to transmit and receive the right signal. By utilizing the correct pulse width, the piezoelectric element is excited at its natural frequency results in the maximum output Table 3.1.

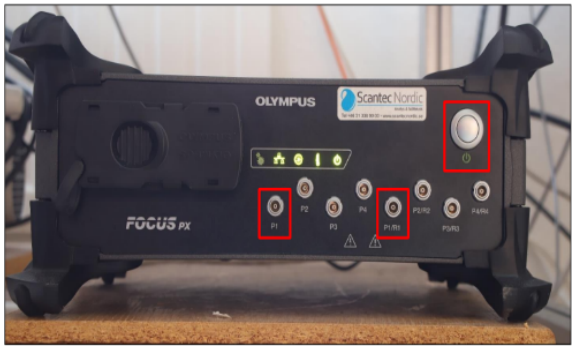

Figure 3.2: Focus PX

Probe Frequency (MHz)	Pulse Width (ns)
2	250
5	100
10	50
15	33
20	32

Table 3.1: Signal pulse width corresponding to probe frequency.

3.1.2 Immersion tank

The immersion tank is an acrylic cylinder 600mm in diameter and 150 mm height with an aluminum bottom. The unit can be set to rotate with a motor control or locked in place. The tank is filled with water via a big watering can and drained by hosing it.

3.1.3 Arm control System (ACS)

The arm can move in 3 linear axes (X, Y and Z), where each axis has a positive and negative directions that is displayed on the frame. Along with that a tilting function with swivel axis in the Y-direction and a fine adjusting mechanism in the Z-direction. Before any controlled movement of the arm must go to a reference position by an action called homing. From the homing position, the motor can move either in a positive or negative direction defined by the software motion task table. Each axis is equipped with motion sensors that stop the arm's movement if it crosses the boundaries. Thus, preventing the arm from hitting the tank walls. The ACS can have 2 axes active at same time, which can be set in two configurations X-Y or X-Z.

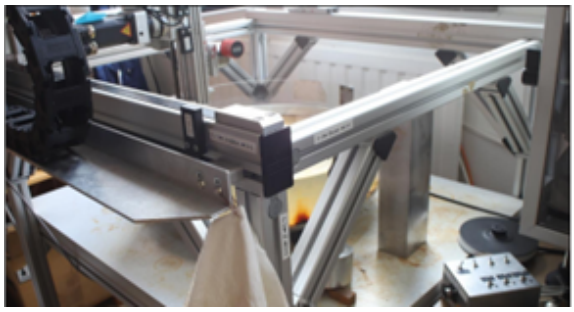

Figure 3.3: ACS axis direction

During the horizontal area scanning, the axes are set in the following motion, the X-axis moves in either positive or negative steps with a minimum length of 0.15mm. The motor can move as far as the motion task table allows it but recommended to stop at 21mm in the X-direction and set the homing position at 20mm step. The Y-axis moves back and forth each forward step in X-axis Figure 3.4.

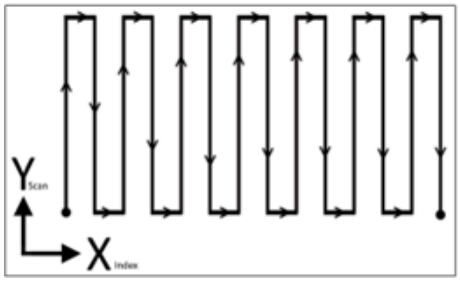

Figure 3.4: Raster Scan Path

The motor has to be enabled before any adjustment or homing, performed by the control box. The control box has 3 main switches for the ACS movement, one for enable to the ACS, second for X-axis movement and Other for Y/Z axis movement.

3.1.4 Encoders

Each of the linear (X, Y and Z), external (L) and rotational (C)axis has a built-in rotational encoder that sends binary signals to the decoder in the Focus PX hardware unit. A rotational encoder connected to a revolving shaft spindle or against a rotating perforated disc under the tank. This perforated disc incorporates position specific holes that allows a laser to pass through, while the receiver reads the signal and translates it into linear motions. Except for X and Y motors, each encoder has their own resolution in terms of steps per mm.

Motor	Encoders
X,Y	204.8 steps/mm
Z	409.6 steps/mm
C	79.293 steps/mm
L	40.0 steps/mm

Table 3.2: Encoder resolutions.

3.2 Phased Array Ultrasonic Testing (PAUT)

PAUT equipment consists of a DAQ hardware -TOPAZ64® from Zetec and an annular phased array probe. TOPAZ64® is a portable 64-channel PAUT equipment equipped with FMC (Full Matrix Capture) and TFM (Total Focusing Method) capabilities. Inspection data from the TOPAZ64® is processed by UltraVision Software. The annular PA probe has frequency of 10MHz with 32 active element and 35mm active diameter and the inter-element spacing of 0.1mm.

3.2.1 Immersion Tank

Plastic immersion tank with dimension 480x300x350 (LxWxH) and the water level is maintained approximately at 170 mm. Here tap water is used as the coupling medium, it should be left alone for more than 24 hours to get rid of air bubbles.

Mechanized Gantry is a motor-controlled system on X-Y plane and manually adjusted in Z axis, which is built on an experimental platform, to ensure a stable inspection. Same as the conventional UT, the encoders control the movement of gantry system.

3.2.2 Mechanised Gantry

To ensure the accuracy and repeatability of our scanning process, a mechanized gantry system was developed and put to use. This specialized system is a bit like a robotic arm. Its designed to help us present our data in different ways, like creating images known as B-scan and C-scan. These images show us what is happening inside the material we're examining.

Then intersting part of this system is that it always knows exactly where our testing tool, or probe, is located. It does this by using special sensors in the motors that move the probe around. So, there is no guessing involved, the system tells us precisely where the probe is at all times.

In the image provided Figure 3.5, shows the mechanized gantry system. It has three parts that can move in different directions, but for our current work, we are only using two of them: the side-to-side movement (X and Y-axes). These movements help us pinpoint the probe's location. The up-and-down movement (Z-axis) is manually adjusted. It aids in gently pressing the probe against the material we are testing.

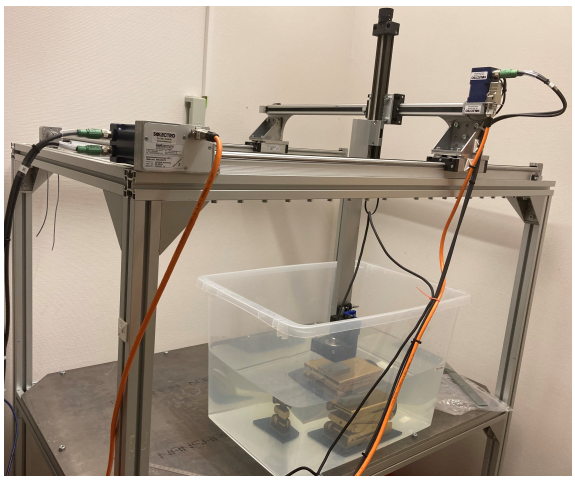

Figure 3.5: PAUT platform with Mechanised Gantry

In straightforward terms, the mechanized gantry system functions like an intelligent robotic arm. It assists in accurately scanning materials and making sense of the data that are collected. It is a vital component of the testing process.

4

Test Specimen

4.1 Test Materials

The test specimens used in this study were printed in two Nickel-based super alloys, specifically alloy 247 and Inconel 939. These alloys were chosen to represent commonly used materials in industries such as aerospace and energy. The specimens were manufactured using the Powder Bed Fusion with Laser Beam (PBF-LB) method at the Siemens Energy, Fingspång.

To evaluate the detection and characterization of defects, the test specimens were intentionally printed with various CAD seeded defects. These defects included side printed holes, internal spheres (IS), penny defects, and spheroidal defects.

- **Alloy 247**

The specimens included four blocks of dimension 120x10x10mm (LxBxH), printed in alloy 247. Two of the blocks were printed with side printed holes, while the remaining two blocks contained internal spheres (IS). Block I and Block II had side printed holes with diameters ranging from 0.05mm to 1.0mm, resulting in a total of 11 defects as shown in Figure 4.1. Block III and Block IV were embedded with IS defects, with diameters ranging from 0.1mm to 1mm, totaling 10 defects as shown in Figure 4.2. Block I and Block III had machined surfaces, while Blocks II and IV were in their as-printed state.

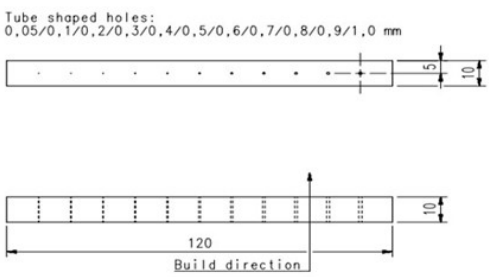

Figure 4.1: CAD design for Alloy 247 Block I and II with printed holes.

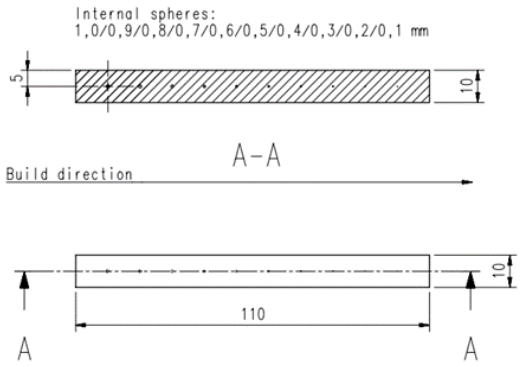

Figure 4.2: CAD design for Alloy 247 Block III and IV with internal spheres.

- **Inconel 939**

In addition to these blocks, 15 blocks of dimension 70x14x14mm (LxWxH) were printed in Inconel 939. These blocks were categorized into five types: Block 1, Block 2, Block 2B, Block 3, and Block 4. Each block type consisted of three sets of samples, resulting in a total of 15 blocks.

Block 1 contained two sets of printed holes, positioned at depths of 14mm and 7mm within the block. These defects in each set had varying diameters of 0.2mm, 0.3mm, 0.4mm, 0.8mm, 1.4mm, 2mm, and 2.6mm,as shown in Figure 4.3.

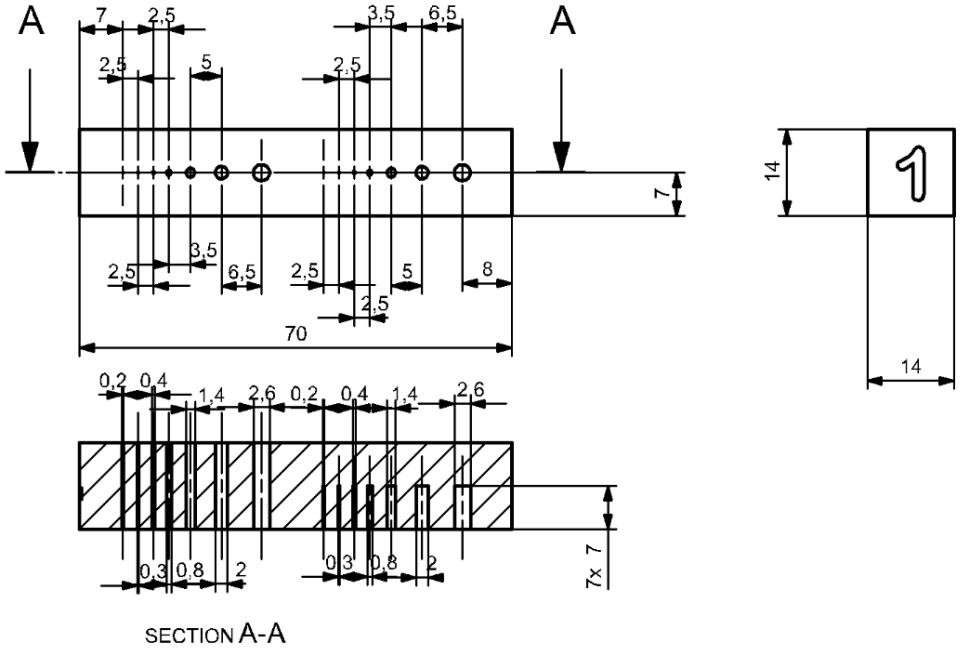

Figure 4.3: CAD drawing of IN 939 block 1 showing side printed holes with diameters.

Block 2 featured penny-shaped defects with 0° roof angles. The defects were divided into three categories: five defects at the extreme end with a defect tilt angle of 0° and dimensions 0.5mm, 1.0mm, 1.5mm, 2.0mm and 2.5mm, five defects in the middle with a defect tilt angle of 45° and dimensions 0.5mm, 1.0mm, 1.5mm, 2.0mm and 2.5mm, and three defects with channels for powder removal, having dimensions of 1.5mm, 2.0mm, and 2.5mm, and a channel width of 1mm, as shown in Figure 4.4.

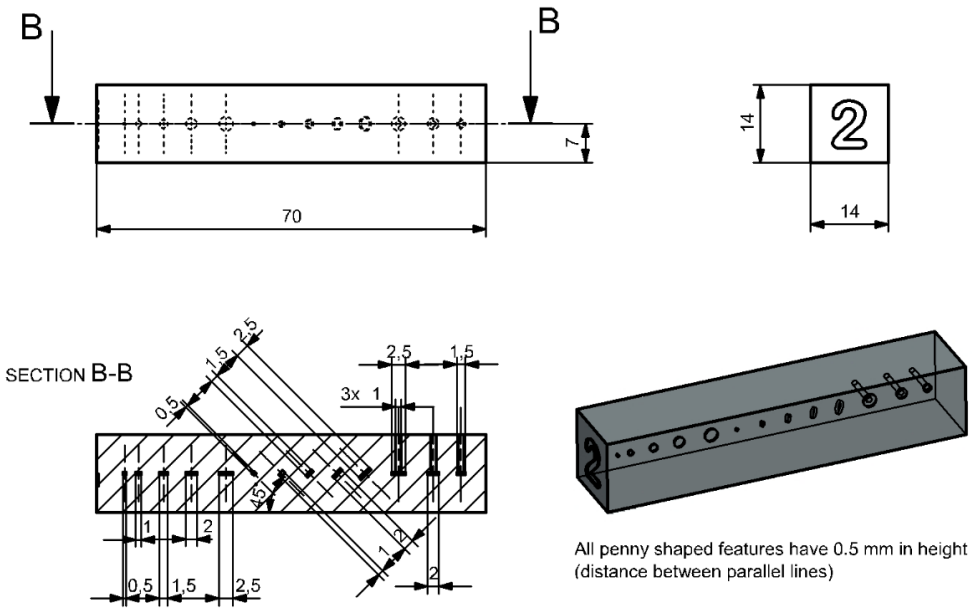

Figure 4.4: CAD drawing of IN 939 block 2 showing Penny defects without roof angle.

Block 2B had the same number and dimensions of penny defects as Block 2, but with a roof angle of 35°. It also consisted of five defects at the extreme end with a defect tilt angle of zero degrees with dimension 0.5mm, 1.0mm, 1.5mm, 2.0mm and 2.5 mm, five defects in the middle with a defect tilt angle of 45° with dimension 0.5mm, 1.0mm, 1.5mm, 2.0mm and 2.4mm, and three defects having dimensions of 1.5mm, 2.0mm and 2.5mm and a channel width of 1mm for powder removal,as shown in Figure 4.5.

Block 3 consisted of 16 internal spheres (IS) arranged within the block. Twelve spheres were positioned in a line at the middle of the block. Six of these spheres were placed on the left side with diameters ranging from 0.5mm to 3mm. Correspondingly, the same defects were mirrored on the right side, with channels defects located on top of these spheres. The remaining four spheres had diameters of 1.5mm, 2.0mm, 2.5mm, and 3mm. These spheres also featured channels with a width of 1mm to facilitate powder removal, as shown in Figure 4.6.

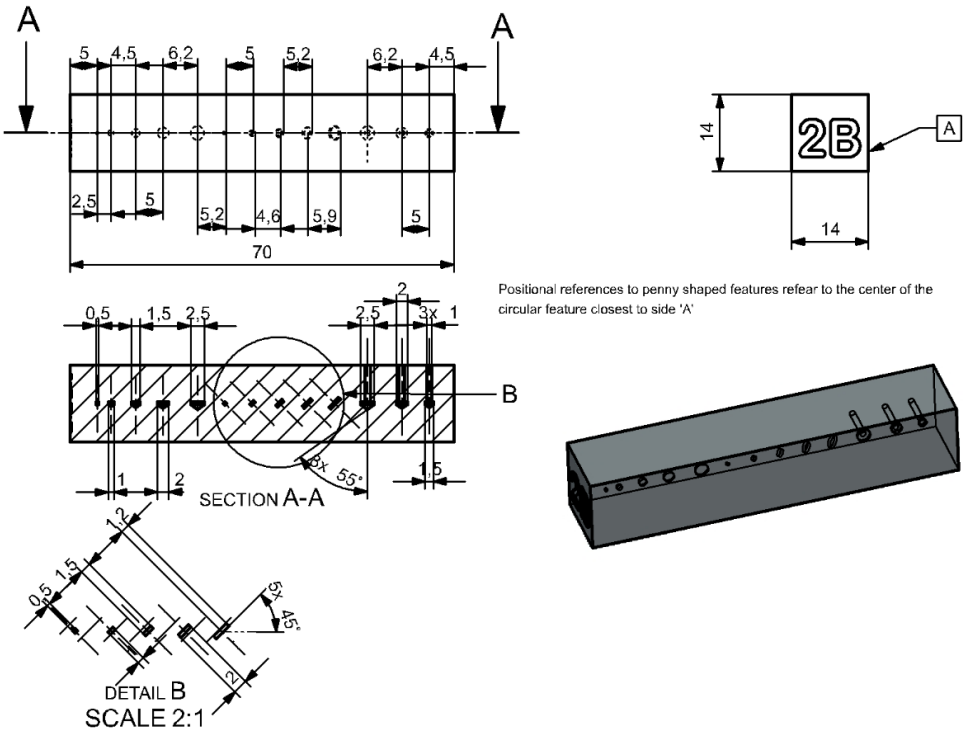

Figure 4.5: CAD drawing of IN 939 block 2B showing side printed holes with diameters Penny defects with roof angle of 35°.

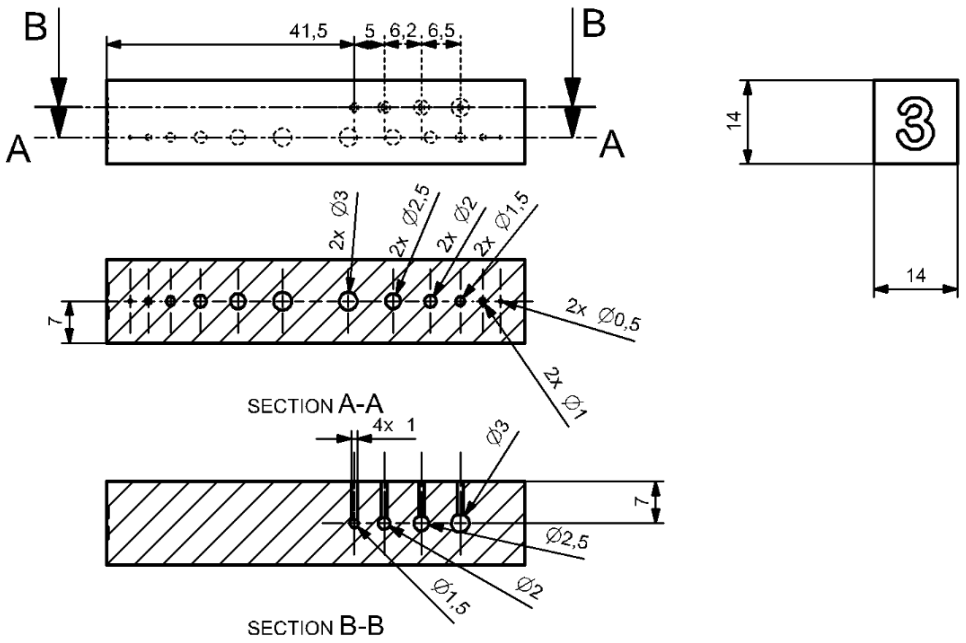

Figure 4.6: CAD drawing of IN 939 block 3 showing internal spheres.

Block 4 consisted of three groups (A, B, and C) of spheroidal defects arranged both vertically and horizontally relative to the built direction. Each group contained four defects with varying dimensions. Group A defects had a major axis of

1.2mm and minor axes measuring 1.0mm, 0.8mm, 0.4mm, and 0.2mm, respectively. Similarly, Group B defects had a major axis of 1.0mm and minor axes measuring 0.8mm, 0.6mm, 0.4mm, and 0.2mm, respectively. Group C defects had a major axis of 0.8mm and minor axes measuring 0.6mm, 0.48mm, 0.32mm, and 0.2mm, respectively, as shown in Figure 4.7.

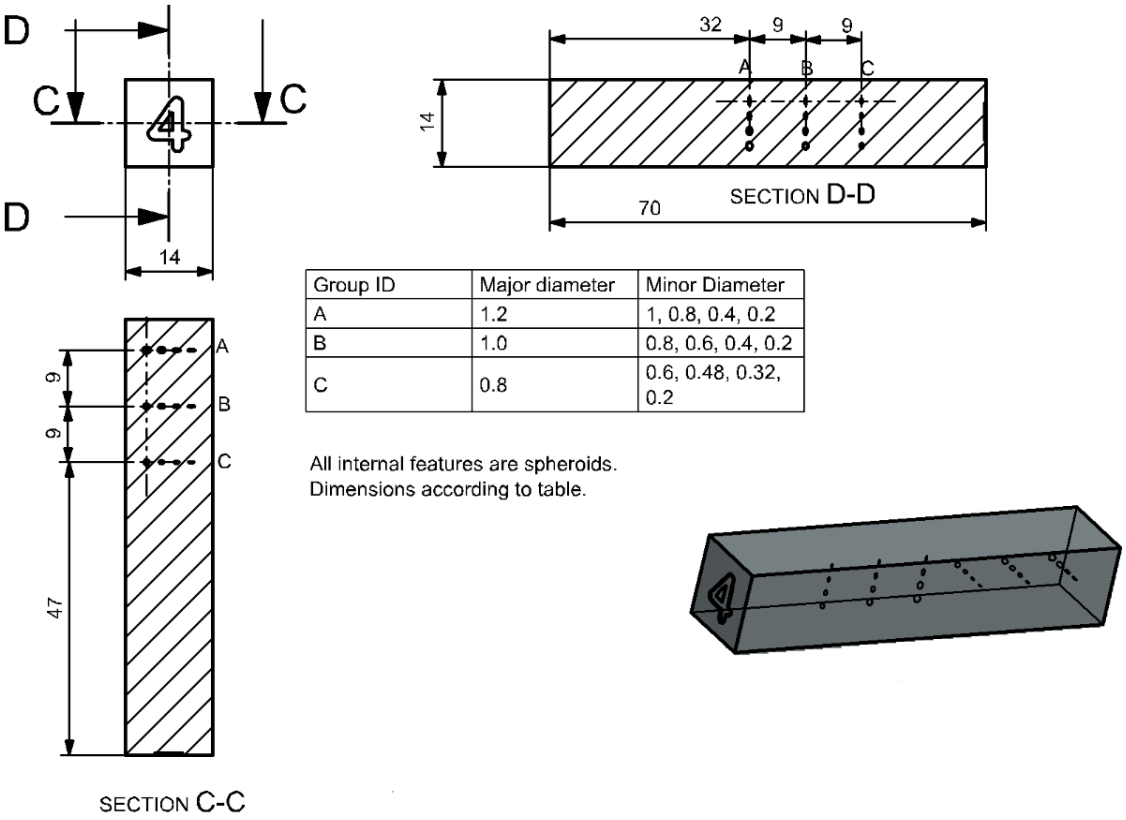

Group ID	Major diameter	Minor Diameter
A	1.2	1, 0.8, 0.4, 0.2
B	1.0	0.8, 0.6, 0.4, 0.2
C	0.8	0.6, 0.48, 0.32, 0.2

Figure 4.7: CAD drawing of IN 939 block 4 showing spheroidal defects.

Similarly, the defects, sizes of defects, defect tilt angle, and defect roof angle of the cylindrical samples are detailed in Table 4.1.

In the inspection process, we employed both Annular Phased Array and conventional Ultrasonic Testing (UT) methods to assess the integrity of the test specimens. The reference defects used for Annular Phased Array inspection included a 1.0mm diameter printed hole in the alloy 247 test specimen and a printed hole with a 2.6mm diameter and 7.0mm depth from block 1 of Inconel 939 test specimen. For conventional UT inspection, a standard reference block with a 1.0mm diameter flat-bottom hole (FBH) at a depth of 5.0mm was employed across all test specimens. The inspection is done on all the as-printed samples and after the inspection, one of the samples are machined and all the inspections are repeated. The design of all the samples is shown in Figure 4.8.

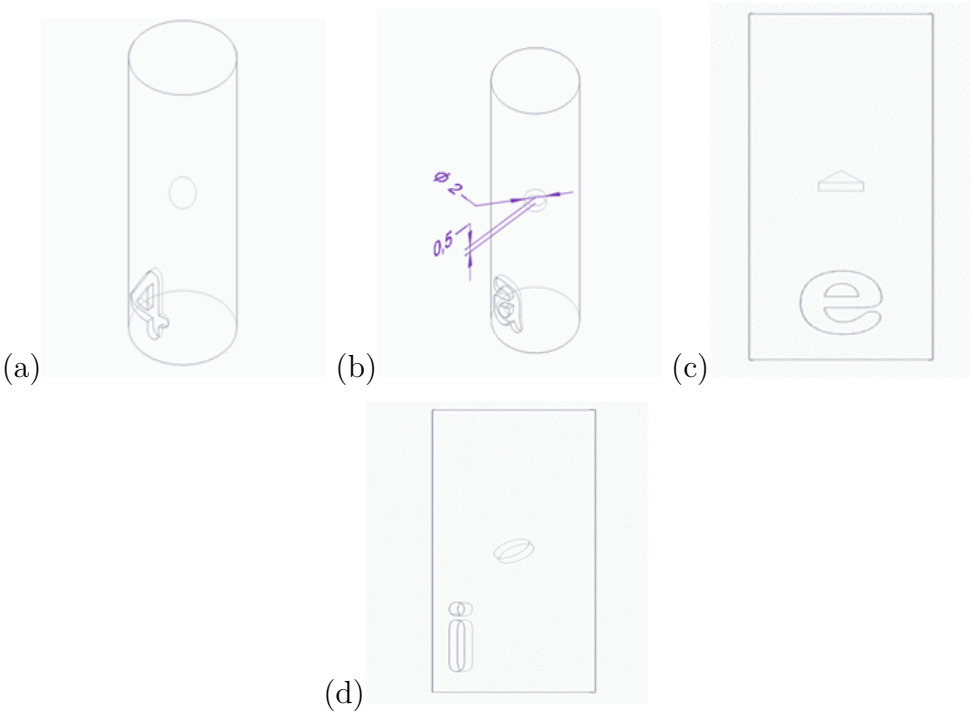

Figure 4.8: CAD design for IN939 cylindrical sample with (a) Internal sphere of defect size of 2 mm, (b) Penny defects with 0° tilt angle with defect size of 2 mm, (c) Penny defects with 0° tilt angle and 35° roof angle with defect size of 2 mm, (d) Penny defects with 45°tilt angle with defect size of 2 mm.

Cylinder ID	Type of Defect	Defect Size (mm)	Defect Tilt Angle (°)	Defect Roof Angle (°)
1	Sphere	0.5	N/A	N/A
2	Sphere	1.0	N/A	N/A
3	Sphere	1.5	N/A	N/A
4	Sphere	2.0	N/A	N/A
5	Sphere	2.5	N/A	N/A
6	Sphere	3.0	N/A	N/A
7	Penny Shaped Defect	0.5	0°	N/A
8	Penny Shaped Defect	1.0	0°	N/A
9	Penny Shaped Defect	1.5	0°	N/A
a	Penny Shaped Defect	2.0	0°	N/A
b	Penny Shaped Defect	0.5	0°	35°
c	Penny Shaped Defect	1.0	0°	35°
d	Penny Shaped Defect	1.5	0°	35°
e	Penny Shaped Defect	2.0	0°	35°
f	Penny Shaped Defect	0.5	45°	N/A
g	Penny Shaped Defect	1.0	45°	N/A
h	Penny Shaped Defect	1.5	45°	N/A
i	Penny Shaped Defect	2.0	45°	N/A

Table 4.1: Dimensions of all the printed defects in IN 939 cylindrical samples.

4.2 Scan Surfaces

The scan surfaces of each block has been marked in the Figure 4.9 . For blocks 1, 3 and 4, the inspection was performed on the as-printed top surface, one of the side surfaces and as-printed bottom surface, shown in Figure 4.9 (a), (d) and (e). For blocks 2 and 2B, the inspection was performed on the as-printed top surface, shown in Figure 4.9 (b) and(c) . The scan and index direction of cylindrical samples are represented in Figure 4.10.

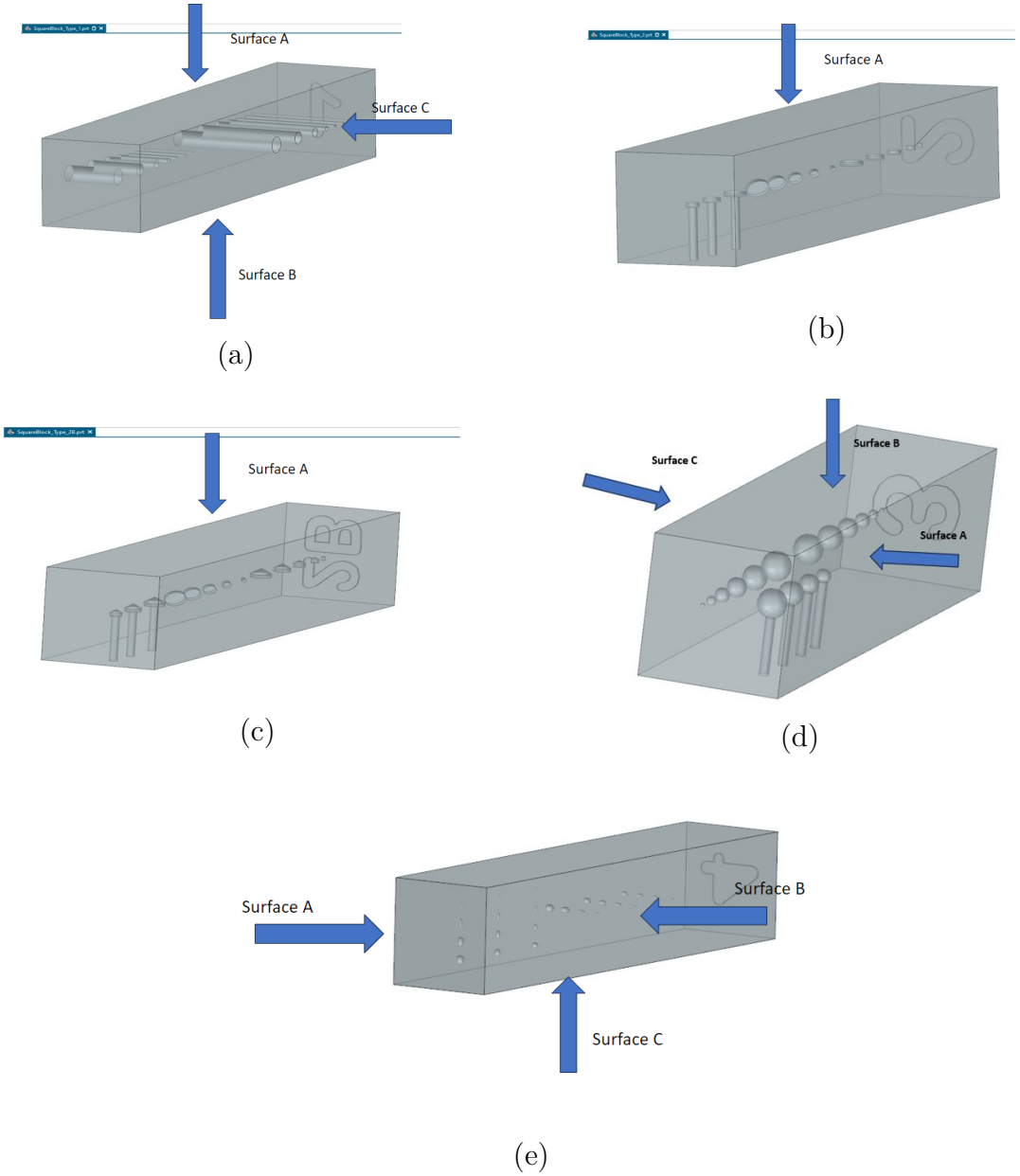

Figure 4.9: CAD design for IN939 sample representing scan surfaces: (a) Block 1, (b) Block 2, (c) Block 2B, (d) Block 3, (e) Block 4.

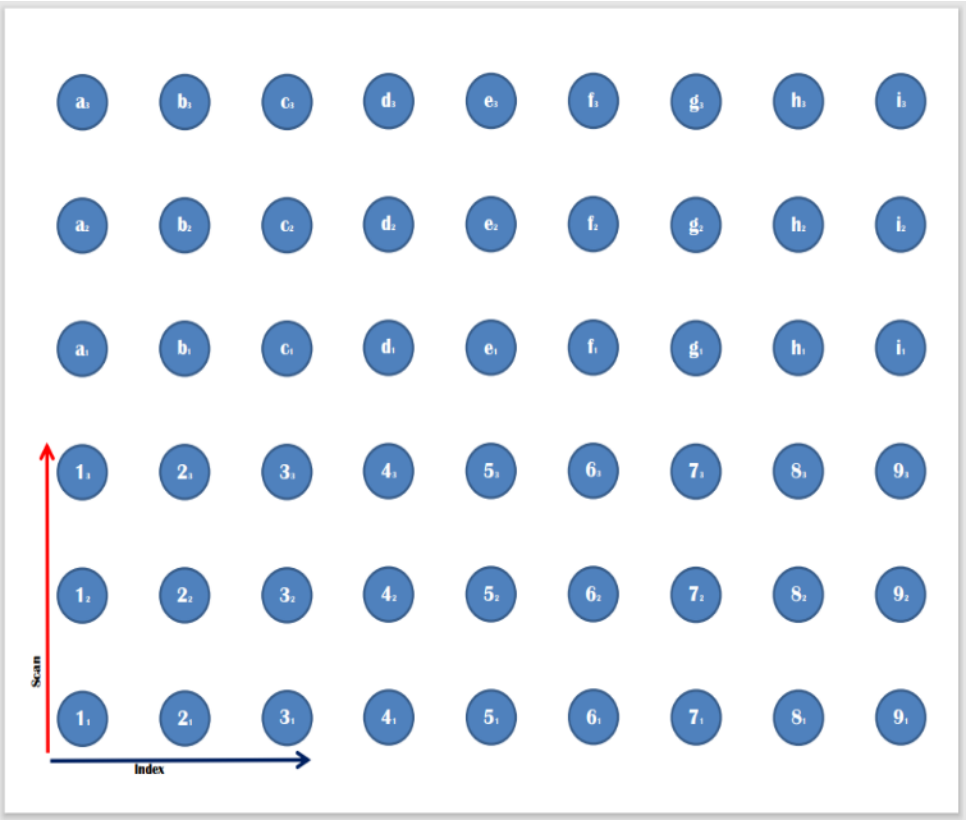

Figure 4.10: Schematic representation of the scan and index directions of IN939 cylindrical samples.

5

Methods and Procedure

5.1 Conventional UT

The mechanized pulse echo ultrasonic testing uses immersion technique having longitudinal waves with 0° refracted angle. The probe operates in pulse echo mode, where one probe acts as both transmitter and receiver of sound waves. In this experiment, the probes used are Harisonic iR1008 with 1.5-inch point focus in water (10 MHz, 0.5- inch diameter), Harisonic iR1008 with 2.5-inch point focus in water (10 MHz, 0.5- inch diameter), Panametrics V327 with 3.25-inch point focus in water (10 MHz, 0.375 -inch diameter. And water is used as the coupling medium. Each probe has a different focal length (F) expressed as the distance between probe surface and focus point measured in water (in inch). The probe with shorter focal length will provide more focused sound beam i.e, smaller focal point diameter, which improves the detectability of the defect and signal-to-noise ratio (S/N).

Two channels are used for the inspection, one for the interface echo and the other for the detection of defects. The interface echo channel should be 10 mm wide, starting from 5mm before the interface echo. The sound velocity in water is taken as 1480m/s. Detection channel range should depend on the test specimen (height of the specimen) and the sensitivity of the interface channel. The validation of all the probes and the reference gain is obtained with the maximum echo amplitude from the cylindrical block with 1mm diameter FBH at 5mm depth, which is presented in the A-scan (detection channel) at the defect position on the test specimen.

Each probe setup has a definite water path (WP) distance between the probe surface and the specimen depending on how deep the focus point should be in the material (depth of the defect). The equation for the water path calculation depends on the sound path into the material i.e, material path (MP) and the focal length of the probe (F), given by

$$WP = F - MP\frac{C_{tm}}{C_w} \tag{5.1}$$

Where,

WP is the one-way water path length.
MP is the one-way sound path to the focus/defect in the material.

F is the focal length in water.
C_tm is the sound velocity in test specimen.
C_w is the sound velocity in water.
C_{tm}/C_w is usually taken as 4.

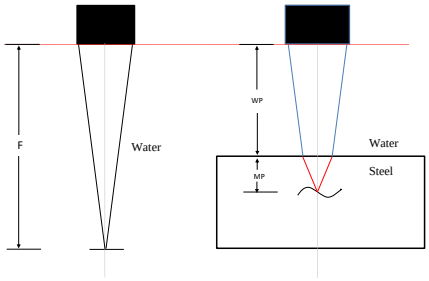

Figure 5.1: Schematic representation of water path (WP) and material path (MP)

The scan and index axis, for all the inspection, for the block samples are shown in Figure 5.2.

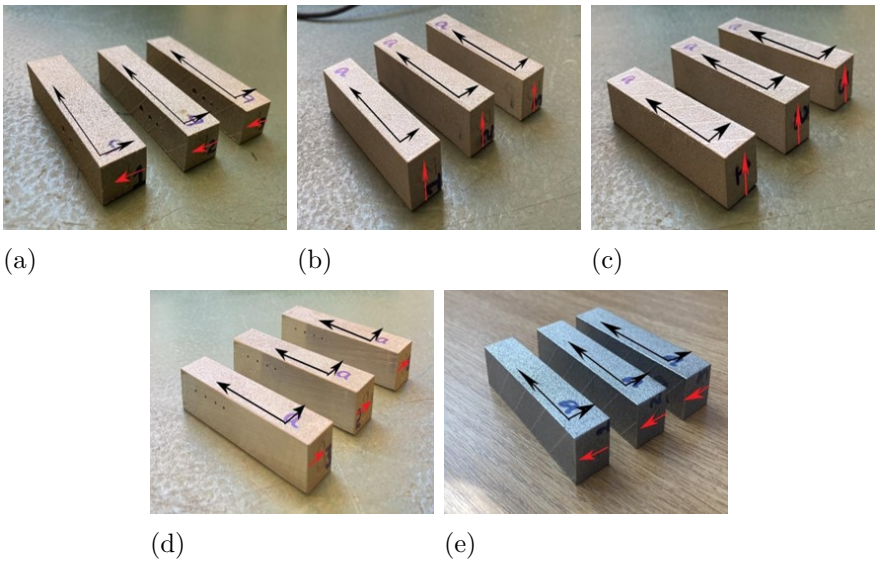

Figure 5.2: Scan and index axis (marked in black) and built direction (marked in red) for (a) Block 1, (b) Block 2, (c) Block 2B, (d)Block 3 (e)Block 4.

In immersion ultrasonic testing, for every scan, first need to find out the reference gain required for inspection. In this work ,the standard reference block with a 1mm diameter flat-bottom hole (FBH) at a depth of 5mm was employed across all test specimens.

The process begins by placing the reference block into the testing tank with suitable water path calculated for each probe. Start the scan and note the gain required to get 100% screen height in the A-scan or detection channel. This gain setting serves as a reference point to help identify defects in the material under examination.

This gain calibration procedure is performed for different probes. Here the reference gain values obtained for two different materials are mentioned below:

- For IN 939 Material:
  For 1.5” probe, the reference gain obtained is 48 dB .
  For 2.5” probe, the reference gain obtained is 49 dB.
  For 3.25” probe, the reference gain obtained is 57 dB .

- For Alloy 247 Material:
  For 2.5” probe, the reference gain obtained is 45 dB.
  For 3.25” probe, the reference gain obtained is 55 dB.

5.2 Phased Array Ultrasonic Testing (PAUT)

The annular phased array (PA) probe operates at a frequency of 10 MHz and features 32 active elements with a 35 mm active diameter. The spacing between these elements is set at 0.1 mm. This particular probe offers the flexibility to adjust and steer the ultrasonic beam, as well as the ability to focus it. For our inspection, we adhere to a minimum water path requirement of 50 mm, as recommended by Zetec. In this work , a water path of approximately 75 mm was maintained . Similarly, in conventional ultrasonic testing (UT), the reference gain is determined using a 2.6 mm diameter through-hole in block 1, as the reference defect, resulting in a reference gain of 26 dB for IN 939.

5.3 X-ray Computed Tomography(XCT)

XCT was performed on selected cylindrical samples containing internal spherical defects of 0.5 mm, 1.0 mm, and 1.5 mm in diameter, as well as penny-shaped defects with a roof angle and a defect dimension of 1 mm. These analyses were performed at the PTC in Trollhättan

The X ray settings for cylindrical samples are:

- Microfocus, 160 kV ; 42 µA

- Filter 0.1 mm Cu + 0.5 mm Sn
- Focal spotsize 6.7 µm
- Voxel size 6.2 µm
- Rotations 2100
- Exposure time 500 ms; Frame averages 7; scan time 75 min.
- Detector shift
- Average SNR at the center of the cylinders 14.3 +/- 0.5 [nodim].

The X ray settings for block 2 samples are:

- Microfocus, 185 kV ; 73 µA
- Filter 0.7 mm Cu
- Focal spotsize 13.5 µm
- Voxel size 13 µm
- Rotations 2000
- Exposure time 250 ms; Frame averages 5 (MID) scan time 1h 15min, 10 (TOP); scan time 2.5 h.
- Detector shift

5.4 Surface Roughness Measurement

The surface roughness was measured using the surface profiler. The roughness is measured using a Mitutoyo equipment ,shown in Figure 5.3 having the probe of 2 (µm) in dimension. Then reference specimen, Figure 5.4 is of dimension 0.5(µm), and the the measurement was done using ISO1997 standard.

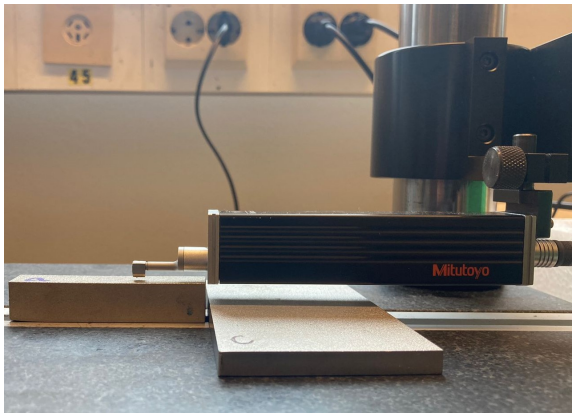

Figure 5.3: Experimental setup showing Surface roughness measurement

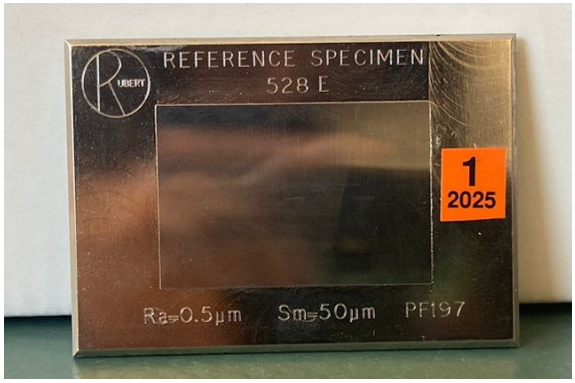

Figure 5.4: Reference specimen for surface Roughness

‘

5.5 Procedure

5.5.1 Procedure for Conventional Immersion Testing

In conventional immersion testing using ultrasonic probes with varying focal lengths, the primary objective is to detect internal discontinuities within test components. The testing is carried out in accordance with EN ISO 16810.

First and foremost, it’s crucial to ensure that the depth of focus at the material matches the known depth of the defect, especially in the case of blocks. The inspection is conducted on both machined and unmachined surfaces of the sample to facilitate the detection of internal discontinuities within the component.

5.5.1.1 References Used:

EN ISO 16810: Non-destructive testing – Ultrasonic testing – General principles.
EN ISO 9712: Non-destructive testing – Qualification and certification of personnel.

5.5.1.2 Testing Technique:

The technique employed is mechanized pulse-echo ultrasonic testing utilizing the immersion method. Longitudinal waves with a 0° refracted angle are utilized.

5.5.1.3 Equipment:

- Instrument
  - Focus PX conventional ultrasonic testing instrument.
- Probe
  - Panametrics V327 with 3.25” point focus in water (10 MHz, 0.375” diameter).

  - Harisonic iR1008 with 1.5” point focus in water (10 MHz, 0.5” diameter).
  - Harisonic iR1008 with 2.5” point focus in water (10 MHz, 0.5” diameter).
- Coupling medium
  - Water.
- Tools
  - Fixtures for mounting the probes in the scanning device.
- Additional equipment
  - Cable for connection of ultrasonic probes and pre-amplifier: Lemo 00 - UHF
  - Cable for connection of encoders to ultrasonic testing instrument

5.5.1.4 Preparation

Ensure that the immersion tank is filled to an adequate level and that the water is clean and without air bubbles. Connect the encoder cables and start the scanning device hard- and software.

- Connection of probe
  - Connect the probe cable to the P1/R1 connector on the instrument.
- Surface preparation
  - The testing surfaces should be free from dirt, corrosion products and other irregularities that can interfere with the testing.

5.5.1.5 Scan and index resolution, scanning speed

During the inspection, the scan and index axes for both the blocks and cylindrical samples are configured as per specifications. It is essential to maintain a scan line interval that does not exceed 50% of the -6 dB beam width at the focal point of the sound field. Additionally, the scanning speed should be deliberately controlled to prevent gaps in the C-scans.

5.5.1.6 Water Path

If the sound path to the discontinuities is known, adjustments to the water path are made to align the focal point with the discontinuities. Notably, probes with shorter focal lengths tend to offer sound beams with smaller focal point diameters, resulting in improved resolution and signal-to-noise ratios. Specifically, for the 1.5” probe, the depth of focus is set at 5 mm. However, for the 2.5” and 3.25” probes, the focus is adjusted to 2 mm for Alloy 939, and 7 mm for both probes in the case of Alloy 247. For cylindrical samples, the depth of focus is standardized at 11 mm. Given these known material paths, the next step involves determining the water path using Equation (1).

For IN939, the calculated water paths for different probes are as follows:

- F1.5” probe: 18.1 mm
- F2.5” probe: 55.5 mm
- F3.25” probe: 74.55 mm

For cylindrical samples, where only probes with 2.5" and 3.25" focal lengths are utilized, the water paths are determined as follows:

- F 2.5" probe: 19.5 mm
- F3.25" probe: 38.55 mm

Similarly, for Alloy 247, the water paths are calculated as follows:

- F 2.5" probe: 43.55 mm
- F 3.25" probe: 63.55 mm

To facilitate the testing process, two channels are utilized: one for the interface echo and another for detection Channel.

5.5.1.7 Probe settings

Fit the probe in the probe fixture. Ensure that the cable is not stretched tight anywhere in the scanning envelope. The baseline settings for the ultrasonic testing are shown in Figure 6.1

General	49 Gain (dB)	3 Start (mm)	12 Range (mm)	6.40 Wedge Delay (us)	LW Wave Type	5890 Velocity (m/s)
Pulser	1 Pulser	PC Tx/Rx Mode	4 Freq (MHz)	300 Voltage (V)	Auto PW (ns)	Auto Max Max PRF
Receiver	2 Receiver	Auto Filter	FW Rectifier	Off Video Filter	1 Averaging	0 Reject (%)
Beam	**Not used**					
Advanced	**Not used**					

Table 5.1: UT settings

5.5.1.8 Range and Sensitivity Setting

The range for the interface echo channel is standardized at 20 mm, commencing 10 mm before the interface echo position. The sound velocity utilized is 1480 m/s.

Sensitivity settings are critical for both the interface echo and defect detection channels. For the interface echo channel, sensitivity is adjusted to ensure that the interface echo amplitude remains below 100 percentage across the scanning envelope.

In the case of the defect detection channel, sensitivity settings are tailored to the specific test object and the presence of backwalls. When a backwall is present, the backwall echo must be considered. The longitudinal sound velocity of the test object material is utilized for sensitivity settings in this channel.

If the soundpath to the discontinuities is unknown, scan the cylindrical reference test pieces using the chosen water path and determine the gain required to have full screen height maximum indication amplitude for each reference test piece. Use the lower of the gain values for scanning of the test objects.

If the soundpath to the discontinuities is known, scan the cylindrical reference test pieces using the chosen water path and determine the gain required to have full screen height maximum indication amplitude for each reference test piece. Use linear interpolation to estimate the gain required to have full screen height maximum indication amplitude at the soundpath of interest, and use this gain for scanning of the test objects.

5.5.1.9 Datas Recorded

The following images are to be prepared:

- C-scan for the defect detection channel.
- B-scan for the defect detection channel.

The following measurements shall be made for each evaluated indication:

- Maximum indication amplitude [dB].
- Sound path at maximum indication amplitude [mm].

5.5.2 Procedure for PAUT

5.5.2.1 General

This procedure describes the technique,equipments ,procedure and reporting for ultrasonic testing of LB-PBF component with up to 15 mm thickness using phase array with immersion technique.The inspection is carried out in the manufacturing stage to detect the internal discontinuities in the component. Testing is to be carried out in accordance with EN ISO 16810. Since a L-PBF component is built up by laser welds, the use of EN ISO 13588 is relevant.

5.5.2.2 References

EN ISO 16810: Non-destructive testing – Ultrasonic testing – General principles EN ISO 13588 : Non-destructive setting of welds– Ultrasonic testing – Use of automated phased array technology EN ISO 18563: Non-destructive testing – Characterization and verification of phased array equipment – Part 3 EN ISO 9712: Non-destructive testing – Qualification and certification of personnel.

5.5.2.3 Testing technique

Automated pulse echo ultrasonic testing using the phased array technique with annular probes. S-scan raster scanning with linear arrays.

5.5.2.4 Equipment

- Instrument.
  - Zetec Topaz 64 phased array instrument.
- Probe.
  - Annular array probe (10 MHz, 32 element, 35 mm active diameter).
- Coupling medium.
  - Water.

- Reference blocks.
  - Standard reference block V1, 1.5mm diameter SDH(printed)at 15mm from the surface.
  - LB-PBF test block with 1mm diameter SDH at 10 mm through hole.
- Tools.
  - Fixtures for mounting the probes in the scanning device.
- Additional equipment.
  - Cable for connection encoders to ultrasonic testing instrument.

5.5.2.5 Preparation

Ensure that the immersion tank is filled to an adequate level and that the water is clean and without air bubbles. Connect the encoder cables and start the scanning device.

- Connection of probe.
  - Connect the probe cable to the instrument.
- Surface preparation.
  - The testing surfaces should be free from dirt, corrosion products and other irregularities that can interfere with the testing.
- Scan and Index resolution, Scanning speed.
  - The interval between two successive scan lines shall be <1 mm. Scanning speed shall be kept low enough to avoid gaps in the data files.
- Probe settings.
  - Fit the probe in the scanning fixture. Ensure that the cable is not stretched anywhere in the scanning envelope.
- Ultrasonic Testing settings

The baseline settings are shown in Table 5.2, Table 5.3 and Table 5.4.

General	26 Gain (dB)	0.00 Start (mm)	12 Range (mm)	0.00 Wedge Delay (µs)	5710 Velocity (m/s)
Pulser	1 Element No.	Negative Square Pulse	50 Pulse Width (ns)	50 Voltage (V)	
Receiver	1 Element No.	Linear Scan Type	None Rectification	None Input Filter	0 Reject (%)
Beam	Not used				
Advanced	Not used				

Table 5.2: PAUT settings

Gate	A6 Gate	Position Parameters	4 Start (mm)	2 Width (mm)	25 Threshold (%)

Table 5.3: Gate Settings

Encoder	1 Encoder	Inverse Polarity	Quad Type	0.15 Resolution (step/mm)	Origin 0 (mm)
Inspection	Area scan Type	Encoder 1 Scan	Off Index	37 Max scan speed (mm/s)	
Foculisation	1 Scan start (mm)	12 Scan end (mm)	0.50 Scan Resolution	Input filter	Reject (%)

Table 5.4: Scan Settings

5.5.2.6 Procedure

In this study, Phased Array Ultrasonic Testing (PAUT) was employed utilizing B-scan, C-scan, and S-scan raster scanning techniques to comprehensively assess the test object. The A-scan channel range was carefully set to 12 mm, initiating at the echo position, with longitudinal sound velocities precisely calibrated at 1447 m/s in water and 5710 m/s in the test block material. Sensitivity adjustments were conscientiously performed to ensure that the echo amplitude remained below 100 % across the entire scanning envelope. For the B-scan, C-scan, and S-scan channels, sensitivity was finely tuned to maintain a 9.80 mm difference between the first echo and the initial backwall echo in the A-scan by precisely adjusting the sound velocity in water. The gain was carefully calibrated to achieve full screen height for the maximum indication amplitude, with the water path adjusted to 76 mm, considering the probe's focal point at approximately 50 mm. Prior to scanning, the alignment of the test block with the gantry was diligently verified by positioning the probe above a sample edge and observing the surface echo in the A-scan channel. The indication amplitude for the 1.5 mm diameter side-drilled hole (SDH) in the V1 block was standardized to 100 % screen height for all focal laws, followed by a deliberate gain increase of 6 dB during scanning to ensure optimal detection sensitivity.

5.5.2.7 Extent of testing

Unless otherwise specified, the entire volume of the test objects was subjected to comprehensive evaluation.

5.5.2.8 Evaluation

Data files from all scanned test objects and test blocks were systematically stored. Unless specified otherwise, any indications with amplitudes exceeding the noise level by more than 6 dB were thoroughly evaluated.

5.5.2.9 Reporting

For each evaluated indication, the following images were prepared:

- A-scan: Captured with a gain setting where the maximum amplitude corresponds to a 1.0 mm side-drilled hole (SDH).
- B-scan: Includes the echodynamic curve for the beam angle that yields the maximum indication amplitude.
- C-scan: Provides a top-down view of the scanned area, illustrating the plan view of the indication.
- S-scan: Acquired at the scan/index position where the maximum indication amplitude is observed for a 1.0 mm diameter SDH, utilizing the 1:1 axis display option.

The following measurements were conducted for each evaluated indication:

- Maximum Indication Amplitude: Measured in decibels (dB).
- Sound Path Length: Determined at the point of maximum indication amplitude, measured in millimeters (mm).
- -6 dB Indication Extension: Assessed in both the scan and index directions, measured in millimeters (mm).

6

Results

6.1 Surface Roughness Measurement for IN939 block

Surface roughness measurement was done on unmachined block 2B and machined block. Both as printed top surface and side surfaces are considered for the measurements. Here in this work only arithmetic mean roughness (Ra) value is measured.

Surface Roughness Measurement (µm)				
	Unmachined Block 2B		**Machined Block 4**	
Ra	**Top Surface**	**Side Surface**	**Top Surface**	**Side Surface**
Ra_1	7.068	6.388	0.159	0.198
Ra_2	6.988	6.337	0.081	0.195
Ra_3	6.883	6.136	0.072	0.202
Ra_4	6.913	6.143	0.064	0.183
Ra_5	6.963	6.089	0.062	0.169

Table 6.1: Surface Roughness Measurements for Inconel 939 sample blocks – Block 2B for unmachined surface roughness and Block 4 for machined surface roughness.

6.2 Conventional Ultrasonic Testing (UT)

The conventional water immersion technique and PAUT with annular probe are used for finding the ultrasonic signal response from printed holes and internal defects in blocks additively manufactured in alloy 247 and IN 939. In conventional UT,the blocks were tested in machined and unmachined as printed surface condition using the probes iwith focus of 1.5", 2.5 "and 3.25". The ultrasonic signal response from the two material indicates that the surface roughness has a significant influence on the detection of defects.Machined surfaces, characterized by lower roughness, consistently facilitated improved ultrasonic signal transmission, yielding clearer and more distinct defect indications.

6.2.1 Alloy 247

The ultrasonic signal responses from both the machined and unmachined surfaces were evaluated using probes with focal lengths of 2.5" and 3.25". These test were conducted to investigate the response characteristics of Blocks I and II. The results of these evaluations are presented in Figure 6.1. A comparative analysis of the responses from the three probes is provided in Table 6.2.

Hole dimension (mm)	1.0	0.9	0.8	0.7	0.6	0.5	0.4	0.3	0.2	0.1	0.05
Machined Probe 3.25"	61	61.5	62	62	63	64	65	65	66	70	70
Unmachined Probe 3.25"	61	63	63	64	64	65	65	65	66	66	66
Machined Probe 2.5"	56	58.5	58	58	59	60	62	64.5	66	66	66
Unmachined Probe 2.5"	59	59	59	59	59.5	59	62	62	62	64	66

Table 6.2: Ultrasonic response from the printed holes in Blocks I and II additively manufactured in Alloy 247.

All printed holes in Alloy 247 Blocks I and II were detectable; however, signal clarity was notably enhanced on machined surfaces. The improved surface finish enhanced the detection and resolution of the ultrasonic scans

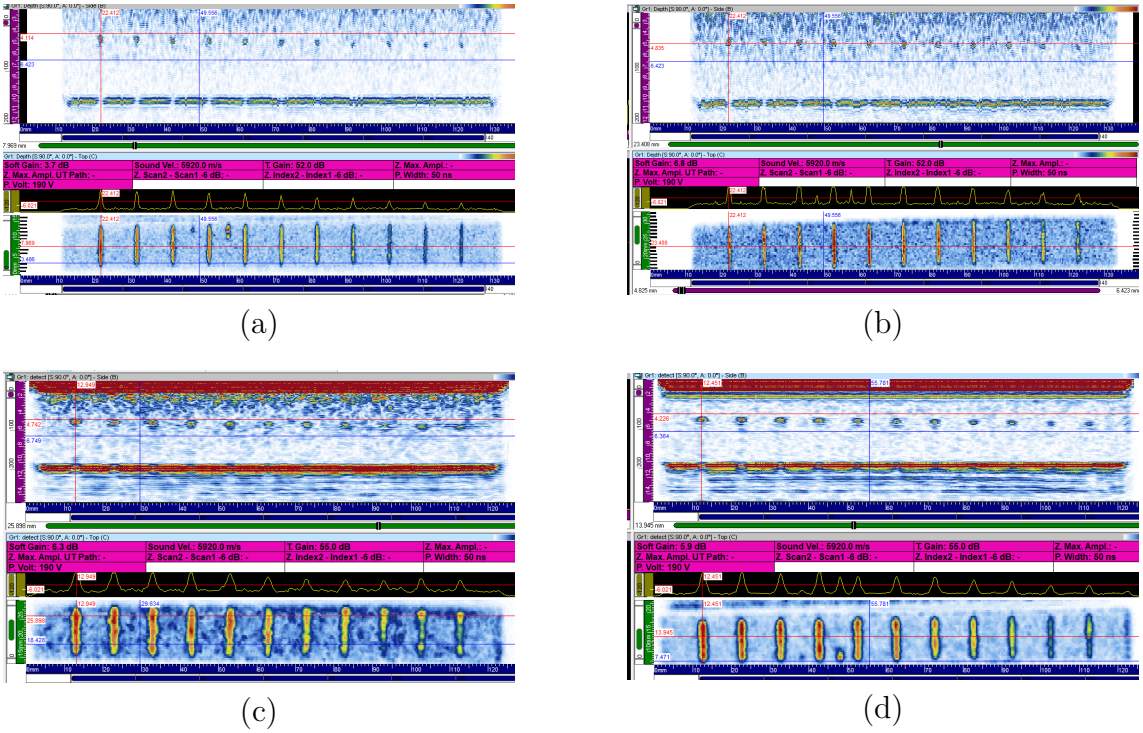

(a) (b) (c) (d)

Figure 6.1: UT results of 1.0 mm printed holes in machined and unmachined Alloy 247 using 2.5" and 3.25" probes in Blocks I and II. (a) Machined, 2.5" probe, (b) Unmachined, 2.5" probe, (c) Unmachined, 3.25" probe, (d) Machined, 3.25" probe. Top: B-Scan; Bottom: C-Scan with echo dynamic curve showing maximum amplitude at the printed hole.

The ultrasonic signal response from the machined and unmachined surface are tested using probes of focus 2.5"and 3.25" are used to find the response of blocks III and IV. And their results are shown in Figure 6.2. The comparison of response form the three probes is shown in Table 6.3.

Defect dimension (mm)	1.0	0.9	0.8	0.7	0.6	0.5	0.4	0.3	0.2	0.1
Machined Probe 3.25"	67	70	73	-	-	-	-	-	-	-
Unmachined Probe 3.25"	-	-	-	-	-	-	-	-	-	-
Machined Probe 2.5"	58	60	63	65	68	69	69	-	-	-
Unmachined Probe 2.5"	-	-	-	-	-	-	-	-	-	-

Table 6.3: Ultrasonic response from the internal spheres in Blocks III and IV additively manufactured in Alloy 247.

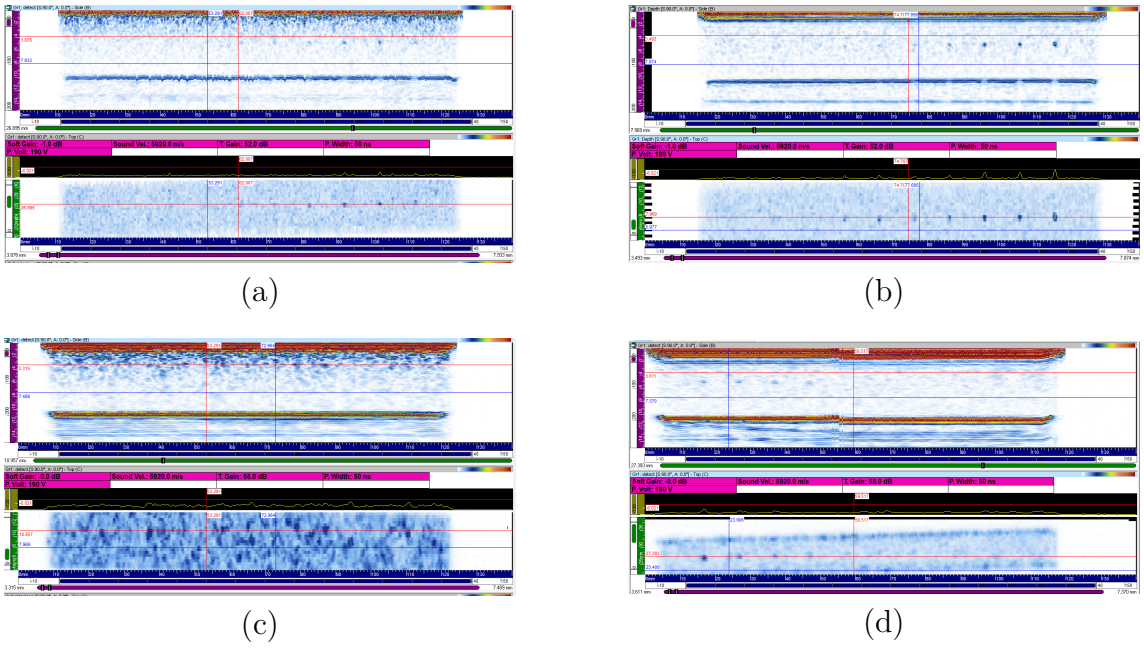

(a) (b) (c) (d)

Figure 6.2: Conventional UT scan results of Alloy 247 internal defects with machined and unmachined surfaces using 2.5" and 3.25" probes in Blocks III and IV . (a) Unmachined, 2.5" probe, (b) Machined, 2.5" probe, (c) Unmachined, 3.25" probe, (d) Machined, 3.25" probe. The top section shows B-Scan results, and the bottom section shows C-Scan results with an echo dynamic curve.

In Alloy 247 Blocks III and IV , it was observed that internal spheres smaller than 0.7 mm were undetectable on machined surfaces when using a 3.25" probe. However, the 2.5" probe successfully detected spheres as small as 0.4 mm on machined surfaces. Spherical defects were not detected on unmachined surfaces, irrespective of probe type, highlighting the critical role of surface finish in ensuring signal integrity. These results highlight the impact of probe focal length and surface finish on detection sensitivity.

6.2.2 Inconel 939

The ultrasonic signal responses from the machined and unmachined surfaces were tested using probes with focal lengths of 1.5", 2.5", and 3.25". A set of three blocks—Block 1, Block 2, Block 2B, Block 3, and Block 4—were printed with various internal defects, including spheres, penny defects, roof angle defects, tilt angle defects, and defects with and without channels, all produced through the PBF-LB process. Scanning was performed on surfaces A, B, and C of the blocks using all three probes, as shown in Figure 4.9. The test data were recorded, and the results are presented in the following sections.

6.2.2.1 Block 1: Ultrasonic Testing on Unmachined or As-Printed Surfaces.

The ultrasonic response of all three samples from Block 1 was evaluated using 3.25", 2.5", and 1.5" probes, with the recorded data presented in Table 6.4 and Figure 6.3. Scanning from surface A, as shown in Figure 4.9(a), successfully detected all defects ranging from 2.6 mm to as small as 0.2 mm. The data indicates that smaller defects require higher energy for detection, as ultrasonic waves need greater intensity to identify them effectively. Additionally, among the three probes, the 3.25" probe exhibited the highest ability to detect smaller defects, followed by the 2.5" and 1.5" probes. This suggests that a larger probe size enhances defect detection, likely due to improved signal penetration and reflection characteristics.

	Maximum Amplitude(dB)-Sample 1.1													
Probe	**Printed 7mm depth hole (0.2-2.6 mm),Gain(dB)**							**Printed 14mm depth hole (0.2-2.6 mm), Gain(dB)**						
	2.6	**2.0**	**1.4**	**0.8**	**0.4**	**0.3**	**0.2**	**2.6**	**2.0**	**1.4**	**0.8**	**0.4**	**0.3**	**0.2**
3.25"	58	61	63	65	66	68	68	59	59	60	64	66	66	67
2.5"	61	63	66	68	71	71	72	61	62	63	66	71	72	72
1.5"	58	61.5	64	67	68.5	69.5	71	58	60	62	65	68.5	70	71
	Maximum Amplitude(dB)-Sample 1.2													
Probe	**Printed 7mm depth hole (0.2-2.6 mm),Gain(dB)**							**Printed 14mm depth hole (0.2-2.6 mm), Gain(dB)**						
	2.6	**2.0**	**1.4**	**0.8**	**0.4**	**0.3**	**0.2**	**2.6**	**2.0**	**1.4**	**0.8**	**0.4**	**0.3**	**0.2**
3.25"	60	61	62	63	66	68	68	59	60	62	65	66	66	68
2.5"	61	61	66	66	70	71	71	60	61	62	66	69	69	71
1.5"	58.5	61.6	62.7	67	69	70	70	57	59	62	65	68	69.5	72.5
	Maximum Amplitude(dB)-Sample 1.3													
Probe	**Printed 7mm depth hole (0.2-2.6 mm),Gain(dB)**							**Printed 14mm depth hole (0.2-2.6 mm), Gain(dB)**						
	2.6	**2.0**	**1.4**	**0.8**	**0.4**	**0.3**	**0.2**	**2.6**	**2.0**	**1.4**	**0.8**	**0.4**	**0.3**	**0.2**
3.25"	58	60	61	62	65	65	66	58	60	61	64	65	66	68
2.5"	60	62	63	65	68	70	71	61	61	63	67	69	68	73
1.5"	56	58	60	62	67	70	70	58	59	61	64	67	69	71

Table 6.4: Ultrasonic response from all samples of Block 1 with unmachined surfaces, scanned from Surface A.

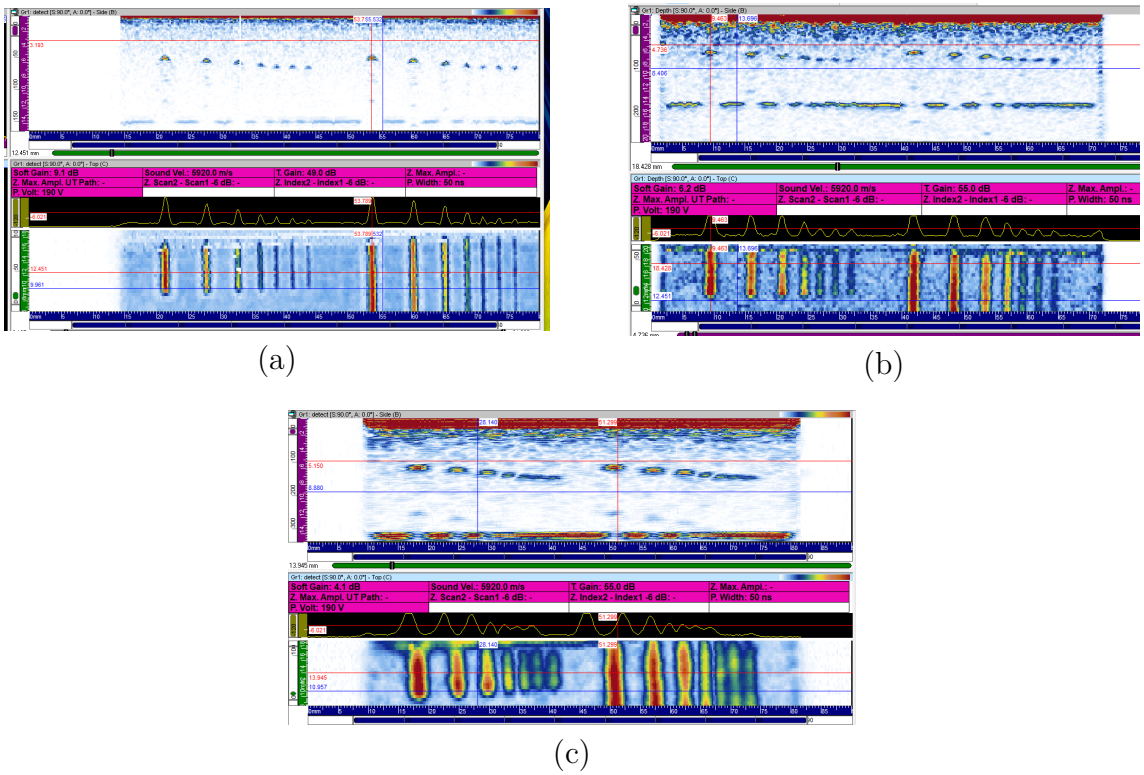

(a) (b)

(c)

Figure 6.3: Ultrasonic response from Block I, Sample 1.1, on the unmachined surface using different probe sizes. (a) 1.5" probe, (b) 2.5" probe, (c) 3.25" probe. The detectability of holes is shown with the B-scan (top window) and the C-scan (bottom window).

6.2.2.2 Block 1: Ultrasonic Testing on Machined Surface.

The ultrasonic response from samples of block 1.2 was tested using probe 3.25", 2.5" and 1.5" and the recorded data was given in Table 6.5. All the defects from 2.6 mm to as low as 0.2mm were detected when scanned from the surface A shown in Figure 4.9(a). The trend of the data shows that, the smaller the hole size the higher the energy required for detectability, Among the three probes, the 3.25" probe demonstrated the highest sensitivity, followed by the 2.5" and 1.5" probes. Ultrasonic testing on machined surfaces yielded superior signal responses compared to their unmachined counterparts.

	Maximum Amplitude(dB)-Sample 1.2													
Probe	**Printed 7mm depth hole (0.2-2.6 mm),Gain(dB)**							**Printed 14mm depth hole (0.2-2.6 mm), Gain(dB)**						
	2.6	**2.0**	**1.4**	**0.8**	**0.4**	**0.3**	**0.2**	**2.6**	**2.0**	**1.4**	**0.8**	**0.4**	**0.3**	**0.2**
3.25"	56	60	64	65	68	68	68	58	59	62	65	66	67	69
2.5"	52	56	57	60	63	64	66	56	55	57	60	64	65	66
1.5"	56	58	62	63	68	68	69	55	57	60	62	66	70	70

Table 6.5: Ultrasonic response from Block 2,sample 1.2, with machined surfaces, scanned from Surface A

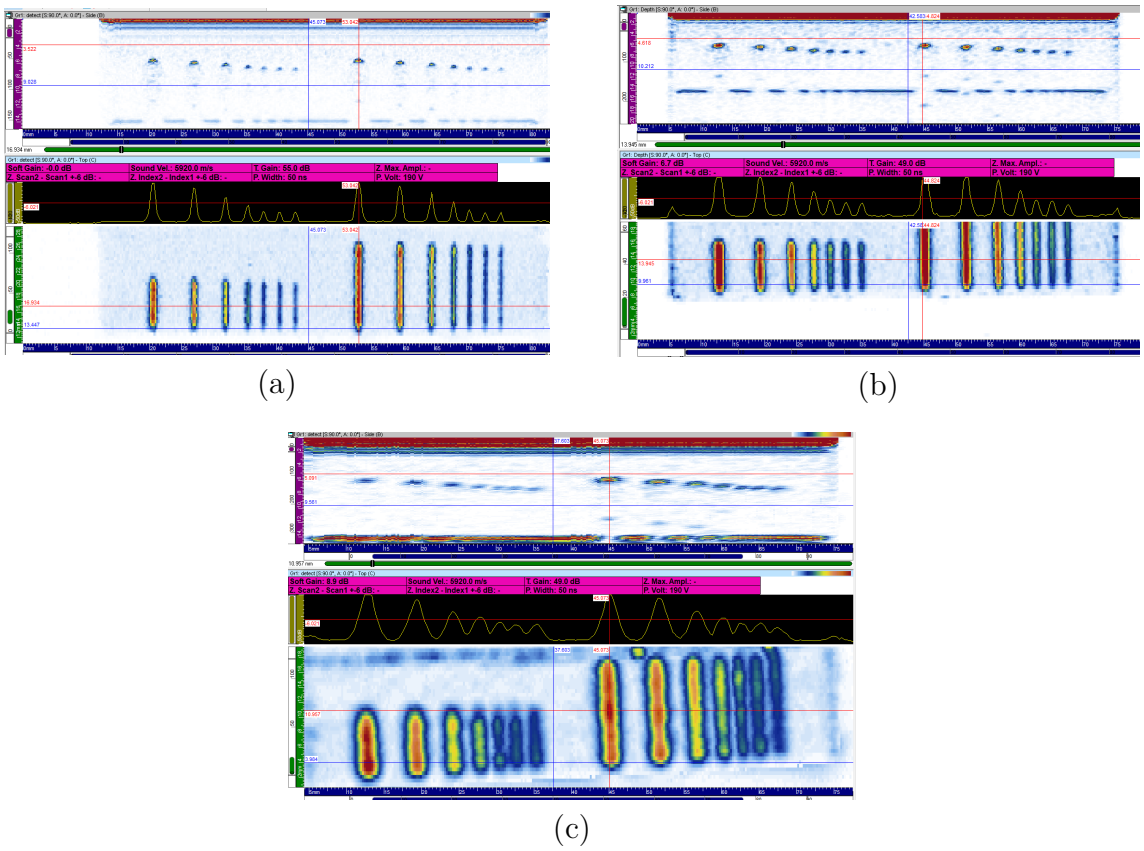

(a) (b)

(c)

Figure 6.4: Ultrasonic response from Block 1, Sample 1.2, machined surface A. The B-scan (top window) and C-scan (bottom window) show hole detection using (a) 1.5" probe, (b) 2.5" probe, and (c) 3.25" probe.

6.2.2.3 Block 2 : Ultrasonic Testing on Unmachined or As-Printed Surfaces.

The ultrasonic evaluation of Block 2 samples was conducted using 3.25", 2.5", and 1.5" probes, with the findings detailed in Table 6.6 and Figure 6.5. All the defects were detected when scanned from the surface A as shown in Figure 4.9(b), successfully identified all defects. The data indicates that while both penny defects with and without channels were identifiable, the detection of defects with tilt angles was limited, with only a few being identified. Notably, the 3.25" probe demonstrated superior sensitivity compared to the 1.5" and 2.5" probes. Additionally, defects without channels showed greater detectability, potentially influenced by the presence of residual powder particles.

	Maximum Amplitude(dB) - Sample 2.1												
Probe	**Penny Defect channel (2.5-1.5 mm)**			**Penny Defect 45° (2.5-0.5 mm)**					**Penny Defect no channel (2.5-0.5 mm)**				
	1.5	**2.0**	**2.5**	**2.5**	**2.0**	**1.5**	**1.0**	**0.5**	**2.5**	**2.0**	**1.5**	**1.0**	**0.5**
3.25"	69	61	61	**THREE detectable**					61	64	67	70	-
2.5"	63	65	71	**THREE detectable**					63	66	70	74	-
1.5"	75	69	67	**Not Detectable**					66	69	73	79	-
	Maximum Amplitude(dB) - Sample 2.2												
Probe	**Penny Defect channel (2.5-1.5 mm)**			**Penny Defect 45° (2.5-0.5 mm)**					**Penny Defect no channel (2.5-0.5 mm)**				
	1.5	**2.0**	**2.5**	**2.5**	**2.0**	**1.5**	**1.0**	**0.5**	**2.5**	**2.0**	**1.5**	**1.0**	**0.5**
3.25"	68	66	61	**THREE detectable**					61	63	67	68	-
2.5"	65	64	64	**THREE detectable**					62	61	67	70	-
1.5"	75	71	68	**Not Detectable**					67	68	71	78	-
	Maximum Amplitude(dB) - Sample 2.3												
Probe	**Penny Defect channel (2.5-1.5 mm)**			**Penny Defect 45° (2.5-0.5 mm)**					**Penny Defect no channel (2.5-0.5 mm)**				
	1.5	**2.0**	**2.5**	**2.5**	**2.0**	**1.5**	**1.0**	**0.5**	**2.5**	**2.0**	**1.5**	**1.0**	**0.5**
3.25"	73	62	63	**THREE detectable**					62	63	65	72	-
2.5"	68	63	61	THREE detectable					62	63	70	71	-
1.5"	73	71	69	Not Detectable					67	71	74	77	-

Table 6.6: Ultrasonic response from all three samples of Block 2 with penny defects (without roof angle), unmachined surface condition, scanned from surface A using 3.25", 2.5", and 1.5" probes.

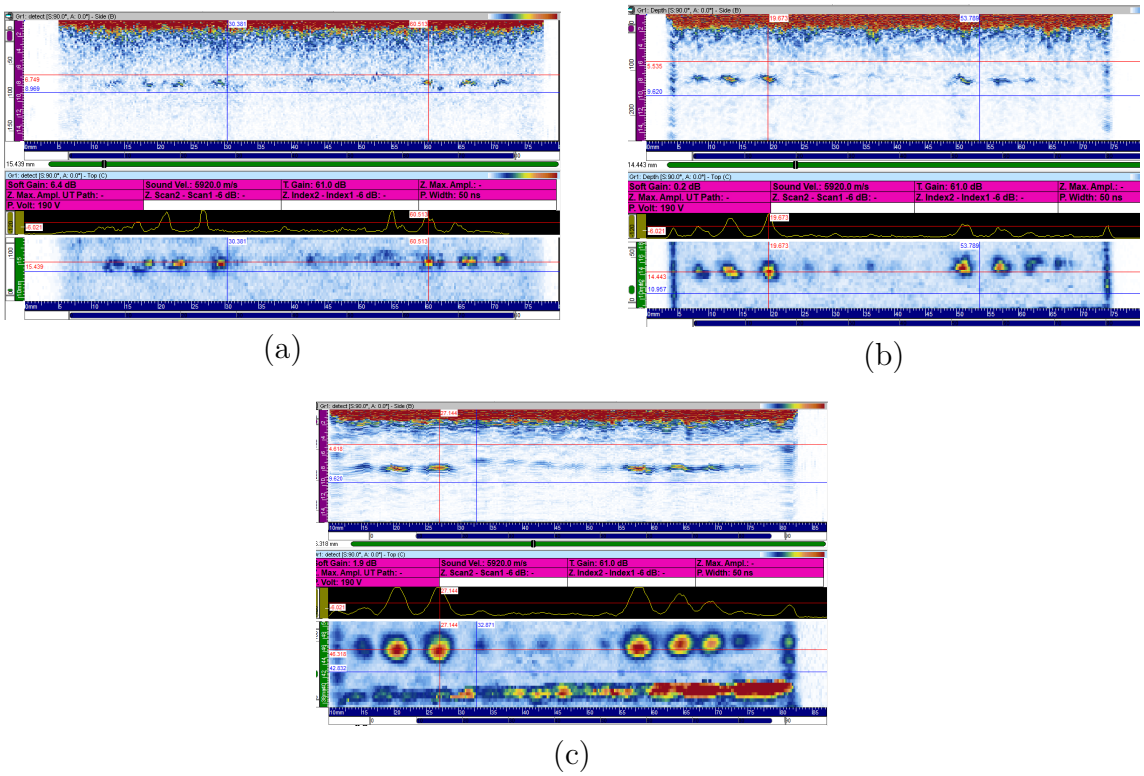

(a) (b) (c)

Figure 6.5: Ultrasonic response from Block 2, Sample 2.1, scanned from unmachined surface A. The B-scan (top window) and C-scan (bottom window) show penny defect detection using (a) 1.5" probe, (b) 2.5" probe, and (c) 3.25" probe.

6.2.2.4 Block 2 : Ultrasonic Testing on Machined Surface

The ultrasonic response from Block 2, Sample 2.3 was evaluated using 3.25", 2.5", and 1.5" probes on the machined surface A, as shown in Figure 4.9(b). The recorded data is presented in Table 6.7 and Figure 6.6. The results indicate that the 3.25" probe successfully detected all types of penny defects, including those with channels, without channels, and with tilt angles. In contrast, defects were difficult to detect using the 2.5" and 1.5" probes. Machined surfaces provided markedly improved ultrasonic responses, particularly in the detection of complex defect geometries.

	Maximum Amplitude(dB) - Sample 2.3												
Probe	**Penny Defect channel (2.5-1.5 mm)**			**Penny Defect 45° (2.5-0.5 mm)**					**Penny Defect no channel (2.5-0.5 mm)**				
	1.5	**2.0**	**2.5**	**2.5**	**2.0**	**1.5**	**1.0**	**0.5**	**2.5**	**2.0**	**1.5**	**1.0**	**0.5**
3.25"	62	60	58	73	73	73	74	76	59	60	61	65	-

Table 6.7: Ultrasonic response from Block 2,sample 2.3 , with penny defects (without roof angle), machined surfaces, scanned from Surface A using a 3.25" probe.

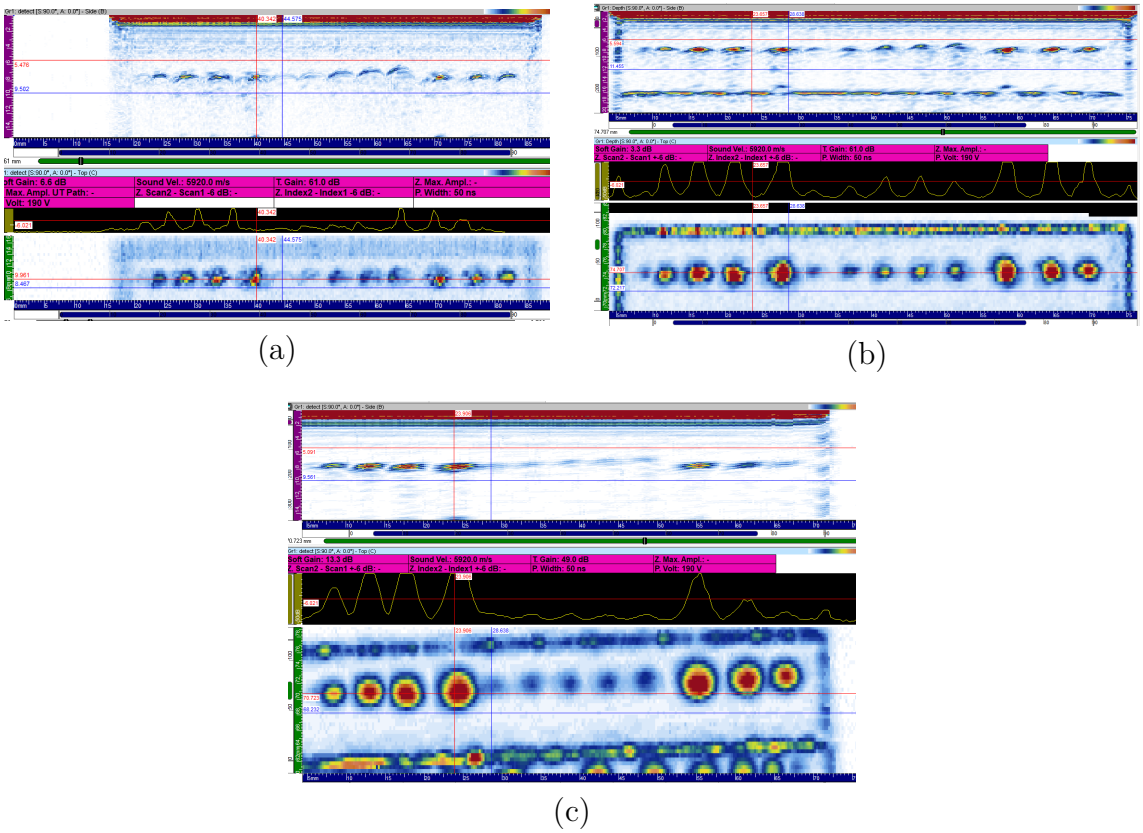

(a) (b) (c)

Figure 6.6: Ultrasonic response from Block 2, Sample 2.3, machined surface A. The B-scan (top window) and C-scan (bottom window) show defect detection using (a) 1.5" probe, (b) 2.5" probe, and (c) 3.25" probe.

6.2.2.5 Block 2B : Ultrasonic Testing on Machined and Unmachined Surfaces.

The ultrasonic response from the samples of Block 2B was evaluated using probes of 3.25", 2.5", and 1.5". The recorded data is presented in Table 6.8 and Figure 6.7. All defects were identified when scanned from surface A, as shown in Figure 4.9(c), which is the as-printed top surface. This block contains penny-shaped defects with varying roof angles, some printed with channels and others without. The data trend reveals that the ability to identify defects was limited by the tilt angle, with only a few defects being detectable. However, when using the 3.25" probe, all defects—both with and without channels—were successfully identified. In contrast, the 1.5" and 2.5" probes failed to detect any of the defects in the block. The 3.25" probe exhibited significantly better detection performance than the 1.5" and 2.5" probes. Performance metrics consistently favored machined surfaces, which exhibited enhanced defect detectability across all probe configurations.

	Maximum Amplitude(dB) - Sample 2B.1												
Probe	**Penny Defect channel (2.5-1.5 mm)**			**Penny Defect 45° tilt angle (2.4-0.5 mm)**					**Penny Defect no channel (2.5-0.5 mm)**				
	1.5	**2.0**	**2.5**	**2.4**	**2.0**	**1.5**	**1.0**	**0.5**	**2.5**	**2.0**	**1.5**	**1.0**	**0.5**
3.25"	68	69	69	68	70	67	-	-	67	-	66	65	-
2.5"	Not Detectable												
1.5"	Not Detectable												
	Maximum Amplitude(dB) - Sample 2B.2												
Probe	**Penny Defect channel (2.5-1.5 mm)**			**Penny Defect 45° tilt angle (2.4-0.5 mm)**					**Penny Defect no channel (2.5-0.5 mm)**				
	1.5	**2.0**	**2.5**	**2.4**	**2.0**	**1.5**	**1.0**	**0.5**	**2.5**	**2.0**	**1.5**	**1.0**	**0.5**
3.25"	68	67	69	68	66	-	-	-	65	66	65	64	-
2.5"	Not Detectable												
1.5"	Not Detectable												
	Maximum Amplitude(dB) - Sample 2B.3												
Probe	**Penny Defect channel (2.5-1.5 mm)**			**Penny Defect 45° tilt angle (2.4-0.5 mm)**					**Penny Defect no channel (2.5-0.5 mm)**				
	1.5	**2.0**	**2.5**	**2.4**	**2.0**	**1.5**	**1.0**	**0.5**	**2.5**	**2.0**	**1.5**	**1.0**	**0.5**
3.25"	68	68	67	65	-	67	-	-	64	65	66	64	-
2.5"	Not Detectable												
1.5"	Not Detectable												

Table 6.8: Ultrasonic response from all three samples of Block 2B with penny defects (with roof angle), unmachined surface condition, scanned from surface A using 3.25", 2.5", and 1.5" probes.

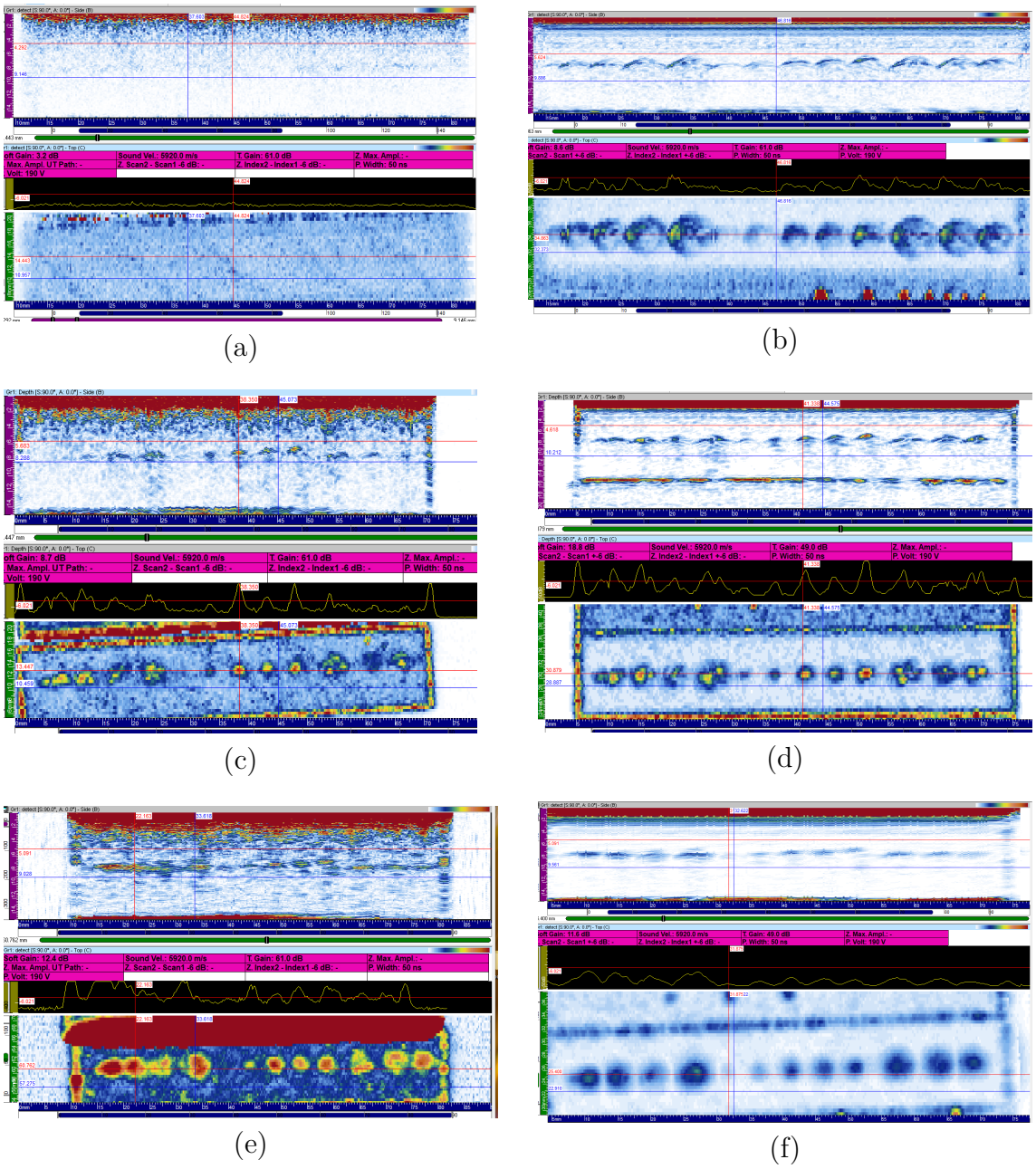

Figure 6.7: Ultrasonic response from Block 2B, with defect detection using various probes: (a) 1.5" unmachined surface, (b) 1.5" machined surface, (c) 2.5" unmachined surface, (d) 2.5" machined surface, (e) 3.25" unmachined surface, and (f) 3.25" machined surface. The B-scan is shown in the top window and the C-scan in the bottom window for all cases.

6.2.2.6 Block 3 : Ultrasonic Testing on Machined and Unmachined Surfaces.

Samples 3.1, 3.2, and 3.3 of Block 3, containing 16 internal spheres (IS), were tested using 3.25”, 2.5”, and 1.5” probes. Twelve spheres were aligned centrally, mirrored on both sides, with channel defects positioned above them; four additional

spheres included 1 mm channels for powder removal. Scans from surfaces A, B, and C (Figure 4.9(d)) revealed limited detectability from surfaces A and C, while surface B showed clearer signals for defects on the right side compared to their mirrored counterparts. The 3.25” probe provided the best detectability. As in previous blocks, machined surfaces yielded clearer signals and more reliable defect characterization. Representative B-scan and C-scan images are shown in Figure 6.8.

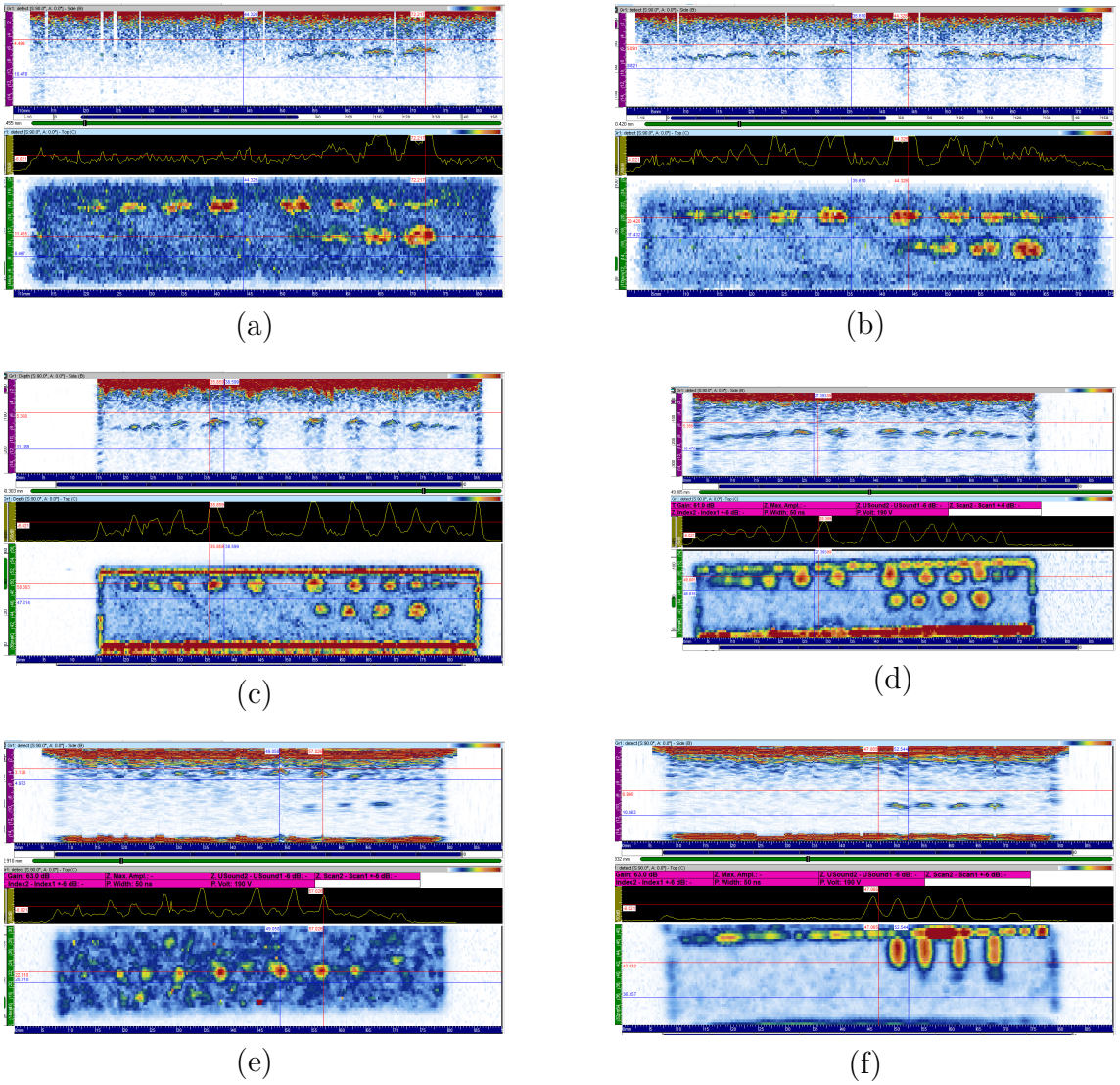

Figure 6.8: Ultrasonic response from Block 3, scanned with various probes and surfaces: (a) 1.5" probe, machined surface (b) 1.5" probe, unmachined surface (c) 2.5" probe, unmachined surface without channel, (d) 2.5" probe, machined surface without channel, (e) 3.25" probe, unmachined surface without channel and (f) 3.25" probe, machined surface without channel. The B-scan is shown in the top window and the C-scan in the bottom window for all cases.

6.2.3 Block 4 with machined and unmachined surfaces

Samples 4.1, 4.2, and 4.3 from Block 4 were tested using 3.25”, 2.5”, and 1.5” probes. Each block contained spheroidal defects arranged vertically and horizontally, printed without internal channels. Scans from surfaces A, B, and C Figure 4.9(e) showed that horizontally aligned defects were best detected from surface A, while vertical ones responded better from surfaces B and C—due to defect geometry. The 3.25” probe offered superior detectability, though defects sized 0.3 mm and 0.2 mm remained undetected due to probe sensitivity limits.

Figure 6.9 presents B-scan (top) and C-scan (side) views from machined and unmachined surfaces. The same defect appears in both scans, with clearer signals and reduced noise on machined surfaces, confirming their enhanced ultrasonic performance.

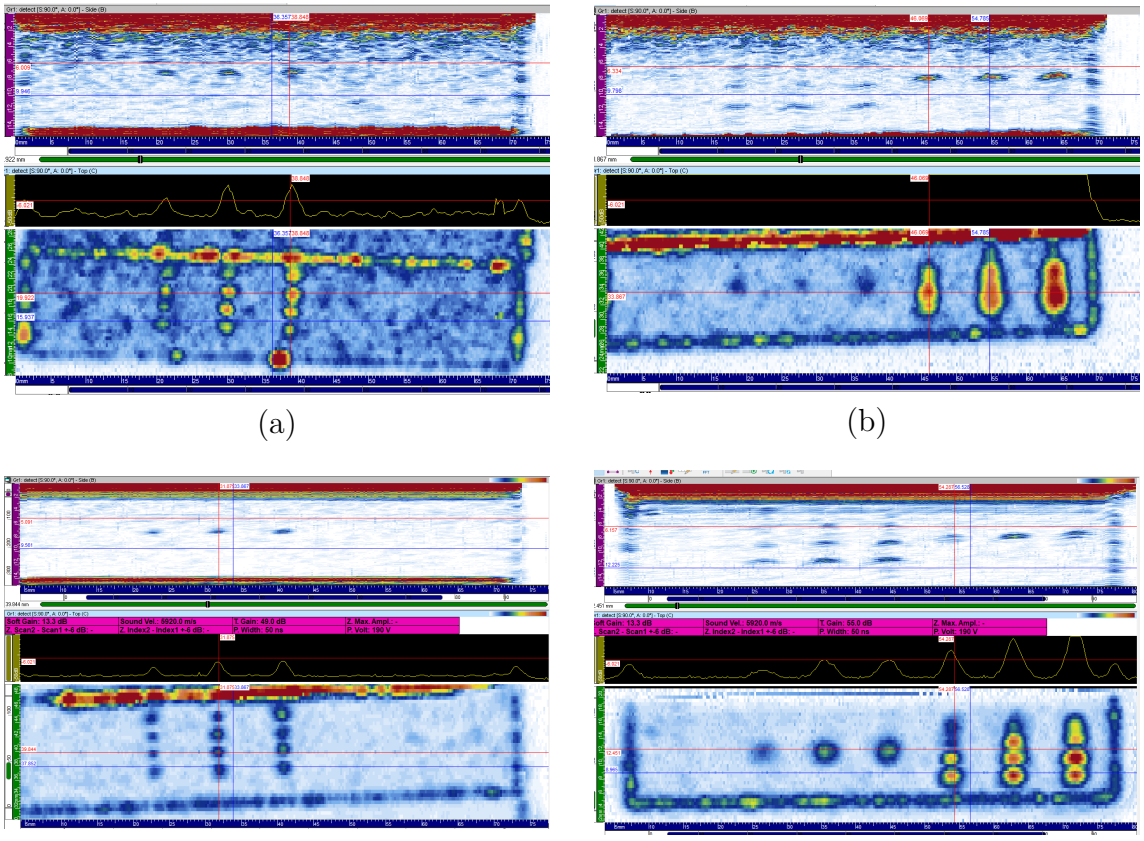

(a) (b) (c) (d)

Figure 6.9: Ultrasonic response from Block 4, Sample 4.1 using a 3.25" probe. The B-scan (top window) and C-scan (bottom window) illustrate defect detection across different surface conditions: (a) and (b) correspond to unmachined surfaces A and C of Sample 4.1, respectively; (c) and (d) represent machined surfaces A and C of the same sample.

6.3 Phased Array Ultrasonic Testing (PAUT)

6.3.1 PAUT response from Alloy 247

The PAUT response of A247 blocks with the machined and unmachined surfaces were tested using different depth of focus from surface A and surface B ,ie from side printed holes and Internals spheres, produced in PBF-LB process. All the defects are detectable when scanned from machined and unmachined surface, with machined surfaces yielding more accurate and distinguishable defect imaging, shown in Figure 6.10.

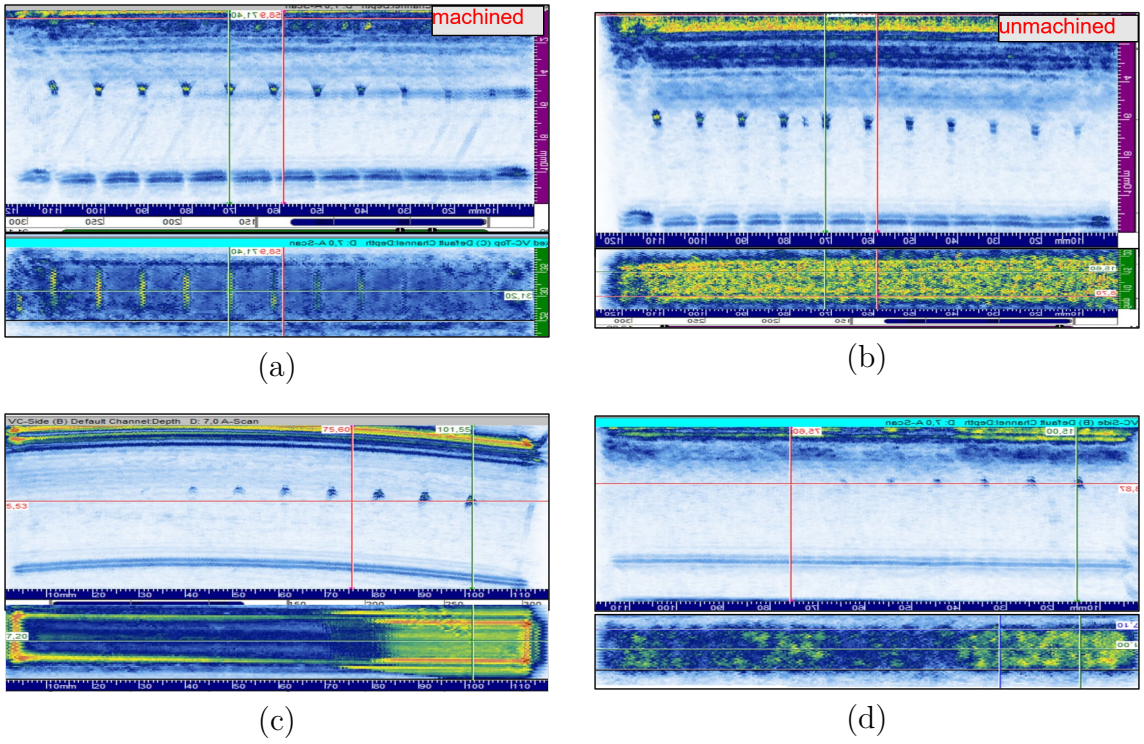

(a) (b)

(c) (d)

Figure 6.10: PAUT response from SDH and Internal Spheres Blocks. The B-scan (top window) and C-scan (bottom window) show defect detection: (a) SDH Block, machined surface, (b) SDH Block, unmachined surface, (c) Internal Spheres Block, machined surface, and (d) Internal Spheres Block, unmachined surface.

6.3.2 IN 939 PAUT response

The PAUT response from the machined and unmachined surfaces of Block 1,2,2B,3 and 4 produced in 3 sets in in PBF-LB process.The blocks produced were printed with internal spheres, penney defects, defects roof angle, tilt angle, defects with channels and without channels for finind the PAUT response. samples were tested using three different depth of focus from surface A, surface B and surface C,Figure 4.9 and the test data was recorded and the results were shown in following sections.All the defects were detectable when scanned from machined and unmachined surface, where smoother surfaces consistently enabled more precise defect

localization and signal clarity.

6.3.2.1 Block 1 machined and unmachined surface

The PAUT response from both machined and unmachined surfaces was evaluated using probes. Block 1 contained two sets of printed holes positioned at depths of 14mm and 7mm, with defect diameters varying across 0.2mm, 0.3mm, 0.4mm, 0.8mm, 1.4mm, 2mm, and 2.6mm. All defects were successfully detected on both surface types; however, machined surfaces exhibited improved defect visibility, shown in Figure 6.11.

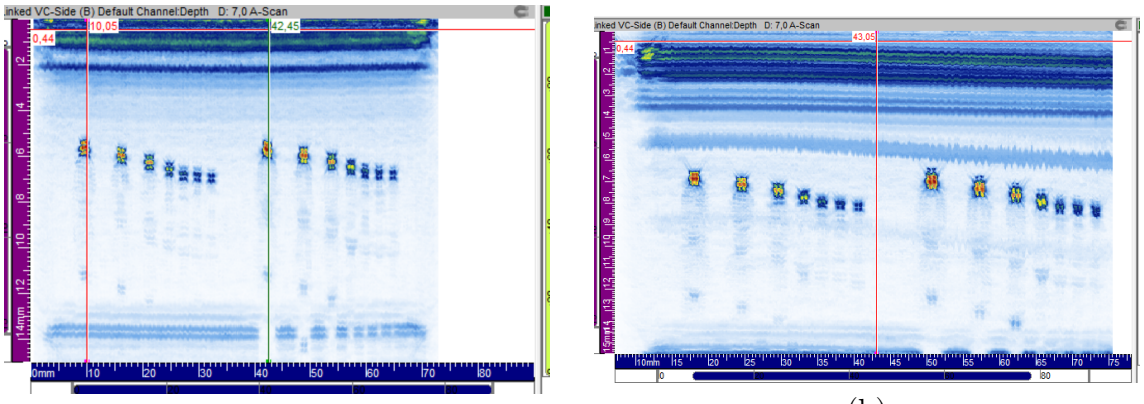

(a) (b)

Figure 6.11: PAUT B-scan results for Block 1 scanned at a depth of 7mm from the top surface: (a) unmachined surface, (b) machined surface.

6.3.2.2 Block 2 Machined and Unmachined Surfaces

The PAUT response from machined and unmachined surfaces was evaluated using probes. Block 2 contained five defects at the extreme end with a defect tilt angle of 0 degrees, five defects in the middle section with a defect tilt angle of 45 degrees, and three defects with channels for powder removal. All defects were successfully detected on both machined and unmachined surfaces. However, machined surfaces demonstrated superior detection accuracy and clarity, improving the overall reliability of the inspection process, shown in Figure 6.12.

	PAUT Maximum Amplitude (dB) - Sample 2												
Sample	**Penny Defect Channel (2.5-1.5 mm)**			**Penny Defect 45° (2.5-0.5 mm)**					**Penny Defect No Channel (2.5-0.5 mm)**				
	1.5	**2.0**	**2.5**	**2.5**	**2.0**	**1.5**	**1.0**	**0.5**	**2.5**	**2.0**	**1.5**	**1.0**	**0.5**
2.1	32	30	30	35	34	34	36	-	30	30	32	34	-
2.2	31	31	30	40	40	40	40	41	30	30	30	34	-
2.3	32	30	30	36	37	39	38	38	29	29	31	32	-

Table 6.9: PAUT B scan results for Block 2 with unmachined surface scanned at a depth of 13 mm from the top surface.

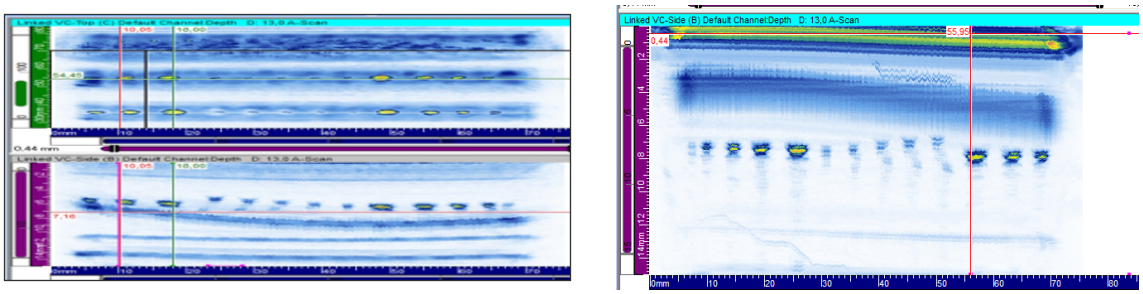

(a) (b)

Figure 6.12: PAUT B-scan results for Block 2 scanned at a depth of 13 mm from the top surface: (a) unmachined surface, (b) machined surface.

6.3.2.3 Block 2B Machined and Unmachined Surfaces

The PAUT response from both machined and unmachined surfaces was evaluated using an annular probe. Block 2B contained five penny defects with a 35° roof angle at the extreme end, oriented at a 0° tilt angle, along with five penny defects in the middle, also with a 35° roof angle but tilted at 45°. Additionally, three penny defects with the same roof angle were present, featuring channels for powder removal. All defects were successfully detected on both machined and unmachined surfaces; however, machined surfaces provided improved clarity as well as precision in defect identification, leading to more accurate and dependable inspection results, shown in Figure 6.13.

	PAUT Maximum Amplitude (dB) - Sample 2B												
Sample	**Penny Defect Channel (2.5-1.5 mm)**			**Penny Defect 45° (2.5-0.5 mm)**					**Penny Defect No Channel (2.5-0.5 mm)**				
	1.5	**2.0**	**2.5**	**2.5**	**2.0**	**1.5**	**1.0**	**0.5**	**2.5**	**2.0**	**1.5**	**1.0**	**0.5**
2B.1	35	33	34	38	37	38	41	41	36	32	32	33	39
2B.2	36	35	36	42	38	40	40	39	35	34	33	36	-
2B.3	37	35	36	36	38	36	40	40	34	35	31	34	40

Table 6.10: PAUT B scan results for Block 2B with unmachined surface scanned at a depth of 13 mm from the top surface.

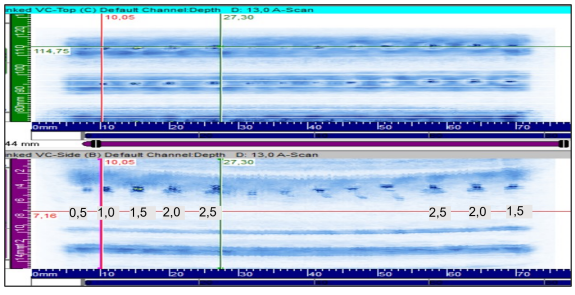

Figure 6.13: PAUT B-scan results for Block 2B with an unmachined surface, scanned at a depth of 13 mm from the top surface.

6.3.2.4 Block 3 and 4 with Machined and Unmachined Surfaces

The PAUT response from machined and unmachined surfaces was assessed using an annular probe. Block 3 contained twelve spheres arranged in a linear configuration at the center of the block. Six spheres were positioned on the left side with diameters ranging from 0.5mm to 3mm, mirrored by an identical set on the right side, where channel defects were located above these spheres. The remaining four spheres had diameters of 1.5mm, 2.0mm, 2.5mm, and 3mm. All defects were successfully detected on both machined and unmachined surfaces; however, machined surfaces demonstrated improved defect visibility and detection accuracy, shown in Figure 6.14.

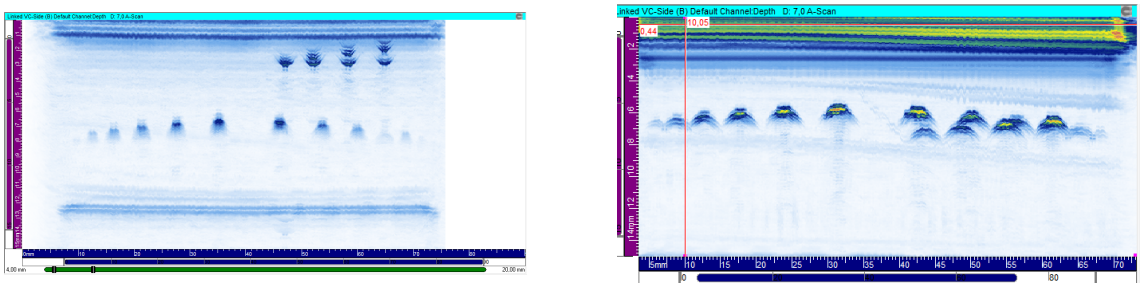

(a) (b)

Figure 6.14: PAUT B-scan results for Block 3: (a) unmachined surface scanned at a depth of 7 mm from Surface A, (b) machined surface scanned at a depth of 7 mm from Surface B.

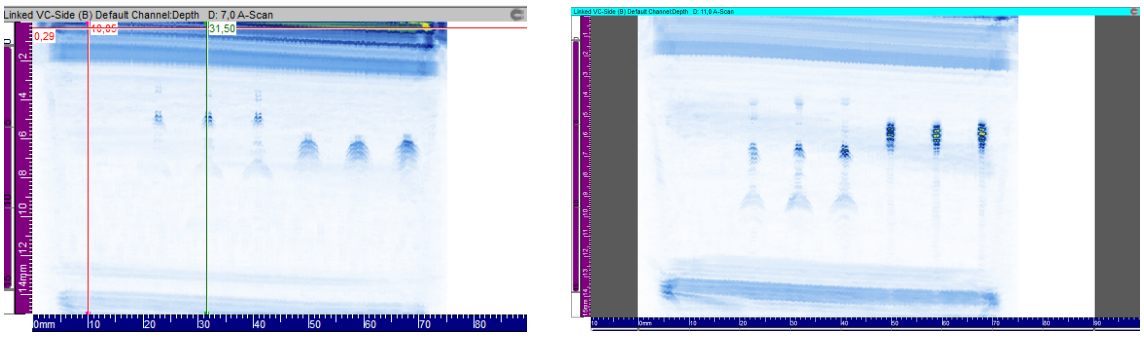

(a) (b)

Figure 6.15: PAUT B-scan results for Block 4: (a) unmachined surface scanned at a depth of 7 mm from Surface C, (b) machined surface scanned at a depth of 7 mm from Surface C.

The PAUT response from the machined and unmachined surfaces was tested using annular probe.Block 4 consisted of three groups (A, B, and C) of spheroidal defects arranged both vertically and horizontally relative to the built direction. Each group contained four defects with varying dimensions. Group A defects had a major axis of 1.2mm and minor axes measuring 1.0mm, 0.8mm, 0.4mm, and 0.2mm,

respectively. Similarly, Group B defects had a major axis of 1.0mm and minor axes measuring 0.8mm, 0.6mm, 0.4mm, and 0.2mm, respectively. Group C defects had a major axis of 0.8mm and minor axes measuring 0.6mm, 0.48mm, 0.32mm, and 0.2mm, respectively . Defects were identified on both surface types, but machined surfaces exhibited greater precision and visibility, shown in Figure 6.15.

6.3.2.5 PAUT for Cylindrical Samples

The PAUT response from the block 2 and cylindrical samples produced in IN939 using PBF-LB process were tested and recorded.In this test 4 sets of cylindrical samples with each set containing 3 samples of 0.5mm,1.0 mm and 1.5 mm internal spherical defects and unmachined block 2 with 3 samples having internal penny shaped defects as shown in Figure 4.8 were used.The test arrangement was shown in Figure 4.10.

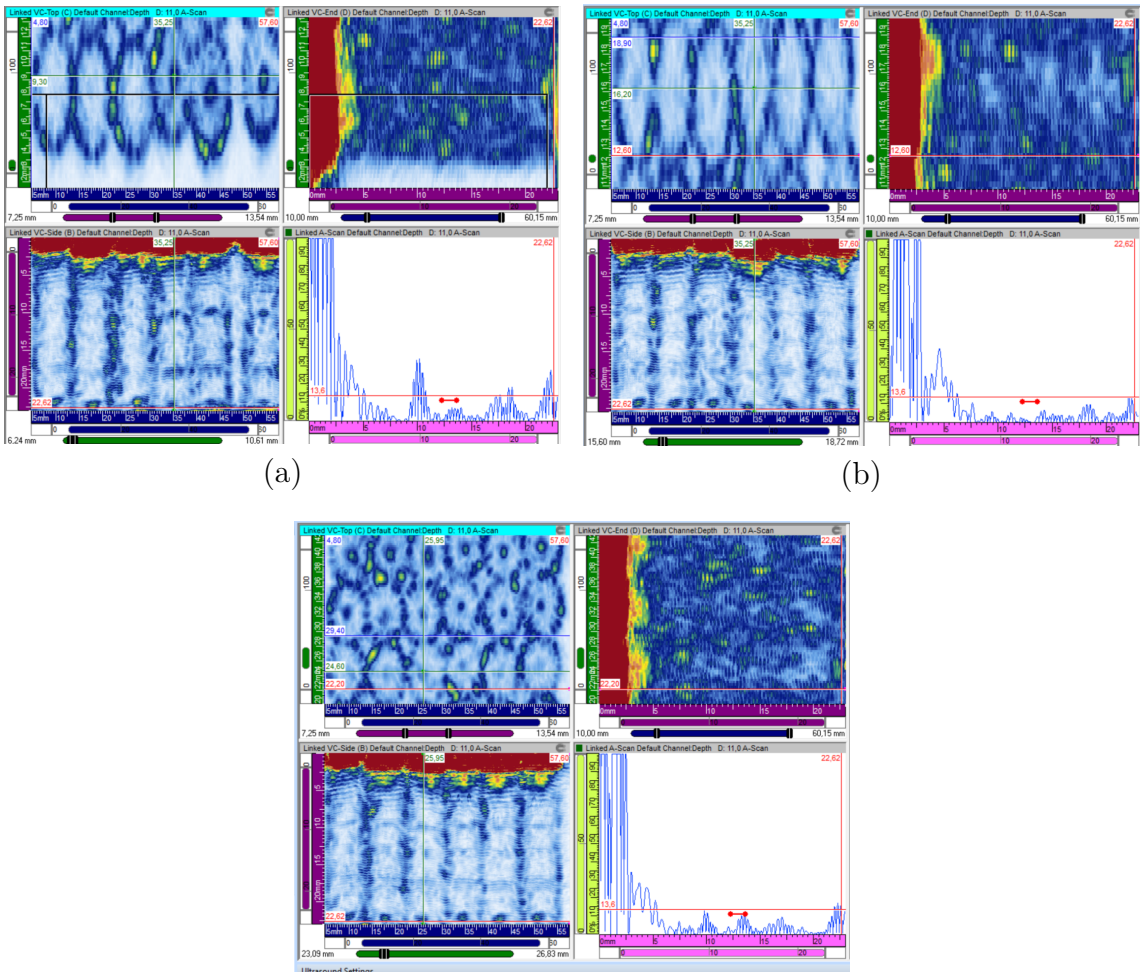

(a) (b)

(c)

Figure 6.16: PAUT results of cylindrical samples: (a) Left 3 cylinders: 0.5mm spherical defects; Right 3 cylinders: 2mm penny defects (b) Left 3 cylinders: 1mm spherical defects; Right 3 cylinders: 0.5mm penny defects (0° tilt, 35° roof angle) (c) Left 3 cylinders: 1.5mm internal defects; Right 3 cylinders: 1mm penny defects (0° tilt, 35° roof angle)

6.4 X Ray Computed Tomography(XCT)

The XCT response from the block 2 and cylindrical samples produced in IN939 using PBF-LB process were tested and recorded, shown in Figure 6.17, Figure 6.18 and Figure 6.19. In this test, 4 sets of cylindrical samples with each set containing 3 samples of 0.5mm,1.0 mm and 1.5 mm spherical defects and unmachined block 2 with 3 samples of penny shaped defects as shown in Figure 4.8 were used.

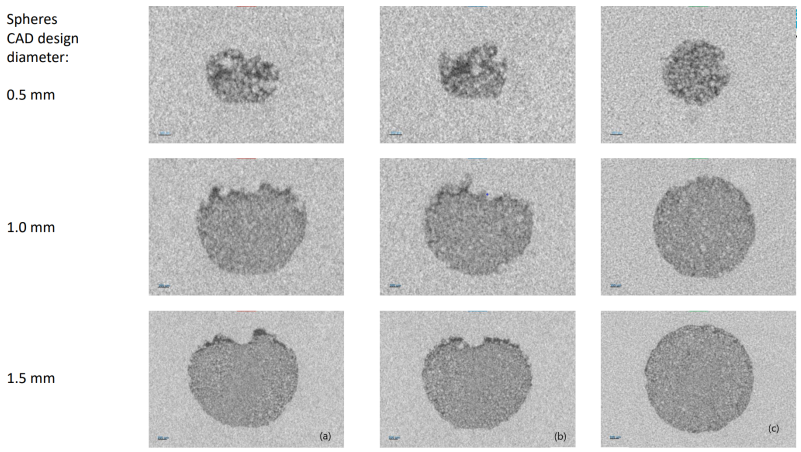

Figure 6.17: XCT slice results for the cylinder having spherical defects of dimension 0.5, 1 and 1.5 mm diameter. Left (a): build direction upwards , Middle (b): build direction upwards in the image, orthogonal plane w.r.t (a) , Right (c): build plane

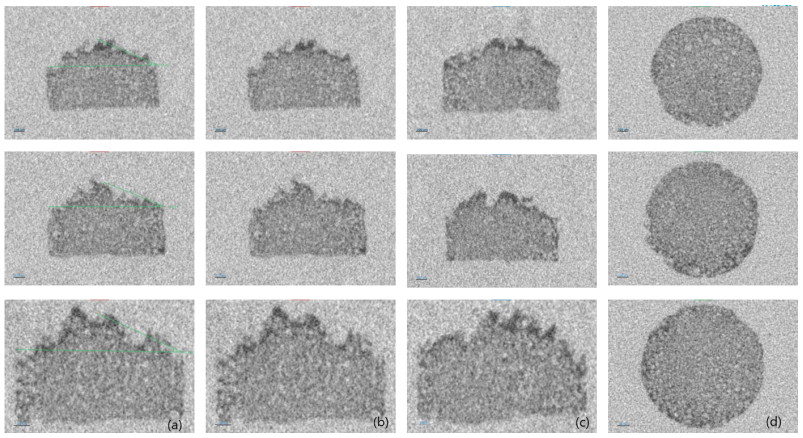

Figure 6.18: XCT slice results for the one set of cylinders having penny defect with 35° roof angle of dimension 1 mm .(a)representing the roof angle of the penny defect, Left (b): build direction upwards , Middle (c): build direction upwards in the image, orthogonal plane w.r.t (a) , Right (d): build plane

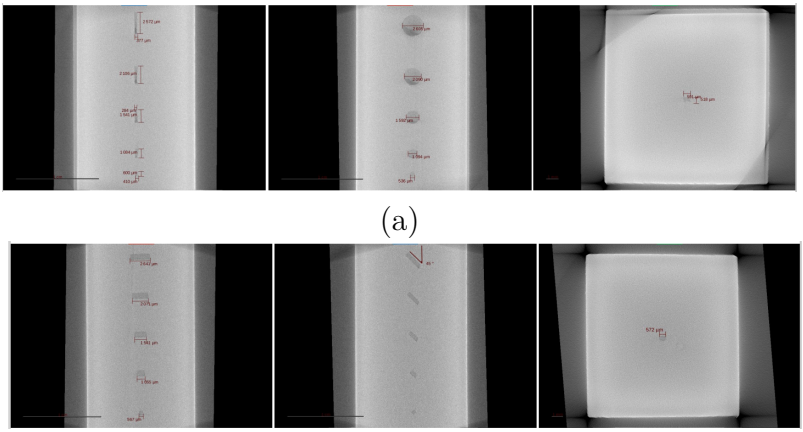

(a)

(b)

Figure 6.19: XCT images illustrating different sections of Block 2.1 with penny defects without roof angle, shown in three orthogonal projections: (a) top section and (b) mid section.

7
Discussion

BLOCK 1: The evaluation of Block 1, which consisted of two sets of printed holes in Blocks 1.1, 1.2, and 1.3 at depths of 7mm and 14mm, aimed to analyze the ultrasonic testing (UT) response and defect recognition under varying scanning conditions. The scanning process was performed using 3.25", 2.5", and 1.5" probes across three different surfaces of the test block, as illustrated in Figure 4.9. A key objective was to assess how different scanning angles influenced defect identification, as well as to compare signal variations between machined and unmachined surfaces. Notably, only Block 1.1 was machined, enabling a direct comparison of signal variance. The results indicate that all holes were successfully detected, with the highest defect recognition observed when using the 3.25" probe on the machined surface. This improved identification on the machined surface may be attributed to reduced scattering and attenuation of UT signals, which are more pronounced on unmachined surfaces. The rough texture of the unmachined surface, produced through the PBF-LB process, is characterized by partially melted powder particles, leading to significant signal interference. This interference, primarily caused by scattering and attenuation phenomena, affects the accuracy and clarity of UT inspection for internal defects. Consequently, the findings highlight the importance of surface finish in ultrasonic testing, demonstrating that machined surfaces provide a more reliable and precise defect detection environment.

BLOCK 2: The block consists of three categories of penny-shaped defects with zero-degree roof angles. These defects were divided into three groups: five defects at the extreme end with a defect tilt angle of zero degrees, five defects in the middle with a defect tilt angle of 45 degrees, and three defects with channels for powder removal. The latter had dimensions of 1.5mm, 2.0mm, and 2.5mm, with a channel width of 1mm. The primary objective was to examine the variability in ultrasonic testing (UT) signals when testing PBF-LB parts containing defects with both unmelted and partially melted powder particles, as well as defects without powder particles. To facilitate particle removal, channels were introduced within the defects, while angled defects were incorporated to assess the effectiveness of UT scanning when defects were oriented at an angle. The test data indicate that both defects with and without channels were successfully identified. However, defects with tilt angles were more challenging to detect due to the probe's limitations in identifying extremely fine defects, further compounded by the impact of the tilt angle itself. Notably, the defects without channels exhibited superior visibility and identification. This trend is likely influenced by the presence of residual powder par-

ticles within the enclosed defects, which may enhance acoustic impedance contrast and improve signal reflection. The assessment of test data and the UT response from Block 2 further reveals that the surface texture of PBF-LB-produced parts significantly influences UT signal responses. Additionally, observations from angled defects highlight that the detection of very fine linear defects is constrained by their size and the probe's sensitivity. . However, penny-shaped defects within PBF-LB-fabricated parts demonstrated consistent detection reliability. This suggests that while nonlinear defects as small as 1mm can be successfully identified, linear defects or those with angular orientations present greater challenges in detection.

BLOCK 2B: The block had the same number and dimensions of penny defects as Block 2 but featured a roof angle of 35 degrees. It contained five defects at the extreme end with a defect tilt angle of zero degrees, five defects in the middle with a tilt angle of 45 degrees, and three defects measuring 1.5mm, 2.0mm, and 2.5mm, along with a 1mm-wide channel for powder removal. The primary goal was to analyze variations in ultrasonic testing (UT) signals when assessing PBF-LB parts with defects containing both unmelted and partially melted powder particles, as well as defects without any residual powder. Channels were incorporated to facilitate powder removal, and the angled defects were introduced to evaluate the feasibility of identifying defects oriented at different angles. The roof angle was specifically included to assess how angular positioning influences the recognition of defects. Test data indicate that defects, regardless of the presence of channels, remained identifiable. However, defects with tilt angles presented challenges due to the probe's limitations in detecting extremely fine flaws, further exacerbated by the influence of the tilt itself. Notably, defects without channels demonstrated superior recognizability. This disparity in flaw perception may stem from the presence of chamfers or sharp edges at the channel interfaces, which can scatter and attenuate sound waves, thereby diminishing flaw identification. Analysis of the UT response from Block 2B underscores the significant impact of surface texture on flaw detection in parts produced via the PBF-LB process. Observations of angled defects highlight that the visibility of exceptionally fine linear defects is constrained by both their size and the sensitivity of the probe. However, penny-shaped defects in PBF-LB-manufactured parts exhibited consistent identifiability. It can be inferred that non-linear defects as small as 1mm are discernible, whereas linear defects or those positioned at an angle demonstrate reduced recognizability. A comparison between Block 2 and Block 2B reveals that penny defects with a roof angle exhibit lower flaw identification rates than those without an angular feature. The 35-degree roof angle likely contributes to increased scattering and attenuation of sound waves, leading to energy loss and necessitating higher dB levels for effective recognition. This effect from the angled surface could also explain why defects with channels are less perceptible than those without. The presence of internal channels within defects may act as additional discontinuities, causing signal interference, dispersion, and attenuation.

BLOCK 3: This block contained 16 internal spheres (IS) arranged within its structure. Twelve of these spheres were aligned in a row at the center of the block. Six spheres were positioned on the left side, with diameters ranging from 0.5mm to 3mm. The same defect pattern was mirrored on the right side, with additional channel defects situated above these spheres. The remaining four spheres had diameters of 1.5mm, 2.0mm, 2.5mm, and 3mm, each featuring a 1mm-wide channel to facilitate powder removal. The primary objective was to assess variations in ultrasonic testing (UT) signals when examining PBF-LB parts with spherical defects that contained both unmelted and partially melted powder particles, as well as defects free of powder. Channels were incorporated within the defects to assist in powder removal and to evaluate the feasibility of identifying spherical defects as small as 0.5mm. Scanning was conducted using 3.25", 2.5", and 1.5" probes from three different surfaces of the test block, as shown in Figure 4.9. The results indicate that flaw recognition was most effective when using the 3.25" probe on a machined surface. The test data also revealed that the defects on the right side appeared more distinctly than those on the left, possibly due to variations in block thickness. In conclusion, the findings suggest that recognizing spherical defects ranging from 0.5mm to 3mm is achievable in parts manufactured through the PBF-LB process.

BLOCK 4: The block consisted of three groups (A, B, and C) of spheroidal defects arranged both vertically and horizontally relative to the build direction. Each group contained four defects of varying dimensions. Group A defects had a major axis of 1.2mm and minor axes measuring 1.0mm, 0.8mm, 0.4mm, and 0.2mm, respectively. Similarly, Group B defects had a major axis of 1.0mm with minor axes of 0.8mm, 0.6mm, 0.4mm, and 0.2mm. Group C defects featured a major axis of 0.8mm and minor axes of 0.6mm, 0.48mm, 0.32mm, and 0.2mm. The primary objective was to evaluate variations in ultrasonic testing (UT) signals when inspecting PBF-LB parts with spherical defects containing both unmelted and partially melted powder particles. Additionally, the study aimed to determine the feasibility of identifying spherical defects as small as 0.2mm, oriented both horizontally and vertically to the scanning surface. Scanning was performed using 3.25", 2.5", and 1.5" probes from three different surfaces of the test block, as shown in Figure 4.9. The results indicated that flaw recognition was most effective when the 3.25" probe was used on a machined surface. Test data revealed that spherical defects as small as 0.4mm could be identified when scanned from a surface perpendicular to the defects. Consequently, it can be concluded that defects of this size are discernible in parts produced using the PBF-LB process. Both conventional ultrasonic immersion techniques and Phased Array Ultrasonic Testing (PAUT) were utilized for assessment. The primary purpose of PAUT was to conduct a comparative analysis with conventional UT. PAUT was applied to all four blocks, and test results confirmed that all defects were successfully identified, even when oriented at an angle. The ability to detect defects using PAUT was found to be superior compared to conventional UT, as expected.

Cylindrical samples were examined using PAUT and XCT to evaluate the response and compare results. The PAUT response from Block 2 and cylindrical

samples produced in IN939 using the PBF-LB process was tested and recorded. In this analysis, four sets of cylindrical samples were used, with each set containing three samples featuring internal spherical defects of 0.5mm, 1.0mm, and 1.5mm. Additionally, an unmachined Block 2 containing internal penny-shaped defects, as illustrated in Figure 4.5 and Figure 4.6, was included. The test setup is depicted in Figure 4.10, and the results are shown in Figure 6.16. The findings indicate that the spherical defects measuring 0.5mm, 1.0mm, and 1.5mm within the cylindrical samples, along with the penny defects, could not be identified using PAUT.

The XCT response from Block 2 and the cylindrical samples produced in IN939 using the PBF-LB process was also tested and recorded. Similar to the PAUT evaluation, four sets of cylindrical samples were analyzed, each containing three samples with internal spherical defects of 0.5mm, 1.0mm, and 1.5mm. Additionally, an unmachined Block 2 with three samples featuring internal penny-shaped defects, as shown in Figure 4.5, was included. The test results are presented in Figure 6.17 to Figure 6.19. The findings reveal that the spherical defects of 0.5mm, 1.0mm, and 1.5mm within the cylindrical samples, as well as the penny defects, were successfully identified. The XCT results were further utilized to measure the dimensions, orientation, and shape of the defects.

8

Conclusion

In this study, five different blocks additively manufactured in IN939 using the PBF-LB process were evaluated using conventional immersion ultrasonic testing. The objective was to assess the feasibility of identifying internal defects in the as-printed condition by analyzing the ultrasonic testing (UT) response from defects with known shapes, sizes, and locations.

The assessment of the test results can be summarised as:

- Defects as small as 0.4mm were consistently identified when positioned perpendicular to the scanning surface. However, defects oriented at an angle or those with a roof angle exhibited reduced visibility due to increased scattering and attenuation of sound waves, particularly on unmachined surfaces.

- The 3.25" probe demonstrated superior performance in defect identification compared to the 2.5" and 1.5" probes. Its wider beam, improved signal-to-noise ratio, reduced near-field interference, and lower sensitivity to surface irregularities contributed to enhanced defect recognition.

- The UT response was significantly improved when scanning was performed on a machined surface. This improvement was attributed to the reduction in scattering and attenuation effects associated with unmachined surfaces.

The objectives of this work were concluded as following:

- This study evaluated defects containing unmelted and partially melted powder particles, as well as defects without powder. The findings indicate that defects without powder exhibited reduced visibility,. This reduction in signal response is likely due to the presence of internal channels designed for powder removal, rather than the absence of powder itself (Figure 6.5-Figure 6.7).

- The presence of melted and partially melted powders significantly impacted the ultrasonic signal response from internal defects. These materials altered acoustic impedance, modified the material structure, and contributed to increased scattering and attenuation, thereby affecting defect detection and characterization accuracy in PBF-LB-produced components.

- Testing was conducted on both as-printed and machined surfaces. The results demonstrated that machined surfaces yielded superior UT responses due to the reduction in sound wave scattering and attenuation caused by partially melted powder particles and the surface texture characteristic of the PBF-LB process.

- Five blocks with different shapes and sizes were analyzed to understand the feasibility and variability of signal responses from internal defects. The results confirmed that defects were more readily identified when oriented perpendicular to the scanning surface. The ability to detect smaller defects was influenced by probe capability and surface condition. Additionally, defects oriented at an angle or those with a roof angle exhibited reduced visibility due to increased signal scattering and attenuation.

- Cylindrical samples were examined using both PAUT and XCT to compare their detection capabilities. The PAUT analysis of the cylindrical samples revealed that defects were not identified, whereas XCT successfully measured defect size and orientation, confirming its effectiveness in defect characterization.

Bibliography

[1] Kumar, R., Kumar, M. and Chohan, J.S., 2021. Material-specific properties and applications of additive manufacturing techniques: A comprehensive review. Bulletin of Materials Science, 44(3), p.181.

[2] Carcreff, E., Laroche, N. and Obaton, A.F., 2023. Review of Ultrasonic Testing for Metallic Additively Manufactured Parts.

[3] Dynamo machine - Stories - Global (siemens.com).

[4] https://www.siemens-energy.com/global/en/home/company/history.html

[5] Additive manufacturing turbines | Siemens Energy Global (siemens-energy.com.

[6] Sames, W.J., List, F.A., Pannala, S., Dehoff, R.R. and Babu, S.S., 2016. The metallurgy and processing science of metal additive manufacturing. International materials reviews, 61(5), pp.315-360.

[7] M.N. Ahsan, R. Bradley, A.J. Pinkerton, Microcomputed tomography analysis of intralayer porosity generation in laser direct metal deposition and its causes, J.Laser Appl. 23 (2) (2011)

[8] Kim, F. H., Kim, F. H., Moylan, S. P. (2018). Literature review of metal additive manufacturing defects (pp. 100-16). Gaithersburg, MD, USA: US Department of Commerce, National Institute of Standards and Technology

[9] Xue, L. and Islam, M. U., "Free-Form Laser Consolidation for ProducingMetallurgically Sound and Functional Components," J. Laser Appl., Vol. 12, 2000,pp. 160 165, https://doi.org/10.2351/1.521927]

[10] A.J. Pinkerton, W. Wang, L. Li, Component repair using laser direct metaldeposition, Proc. IMech Part B – J. Eng. Manuf. 222 (2008) 827–836.].

[11] Consonni, M., Howse, D., Wee, C. F., and Schneider, C., "Production of Joints Welded with Realistic Defects," Weld. Int., Vol. 28, No. 7, 2013, pp. 535–546,

[12] Crutzen, S., Lemaitre, P., and Iacono, I., "Realistic Defects Suitable for ISI (in Service Inspection) Capability Evaluation and Qualification," presented at the 14th International Conference on NDE in the Nuclear and Pressure Vessel Industries, Stockholm, Sweden, Sep. 24–26, 1996, ASM International, Materials Park, OH, pp. 153–163

[13] Everton, S.K., et al.: Review of in situ process monitoring and in situ metrology for metal additive manufacturing. Mater. Des. 95, 431–445 (2016)

[14] Cerniglia, D., Montinaro, N.: Defect detection in additively manufactured components: laser ultrasound and laser thermography comparison. Proc. Struct. Integr. 8, 154–162 (2018)

[15] Chua, Z.Y., Ahn, H., Moon, S.K.: Process monitoring and inspection systems in metal additive manufacturing: status and applications. Int. J. Precis. Eng. Manuf. Green Technol. 4(2), 235–245 (2017)].

[16] A.Thompson, I. Maskery, R.K. Leach, X-ray computed tomography for additive manufacturing: a review, Meas. Sci. Technol. 27 (7) (2016) 072001.
[17] M. Aminzadeh and T. R. Kurfess, "Online quality inspection using Bayesian classification in powder-bed additive manufacturing from high-resolution visual camera images," Journal of Intelligent Manufacturing, pp. 1-19, 2018]
[18] L. Pejryd, P. Karlsson, S. Hällgren, and M. Kahlin, "Non-destructive evaluation of internal defects in additive manufactured aluminium," in European Congress and Exhibition on Powder Metallurgy. European PM Conference Proceedings, 2016: The European Powder Metallurgy Association, pp. 1-7.
[19] Waller, J.M., et al.: Nondestructive Evaluation of Additive Manufacturing State-of-the-Discipline Report. National Aeronautics and Space Administration, Las Cruces (2014)
[20] Dewulf W, Tan Y and Kiekens K 2012 Sense and non-sense of beam hardening correction in CT metrology CIRP Ann. Manuf. Techn. 61 495-8
[21] Palanisamy, S., Nagarajah, C.R. and Iovenitti, P., 2007. Ultrasonic inspection of rough surface aluminium die castings. Insight-Non-Destructive Testing and Condition Monitoring, 49(3), pp.160-164.
[22] Simonetti, F. and Fox, M., 2019. Experimental methods for ultrasonic testing of complex-shaped parts encased in ice. NDT E International, 103, pp.1-11.
[23] Simonetti, F., Satow, I.L., Brath, A.J., Wells, K.C., Porter, J., Hayes, B. and Davis, K., 2018. Cryo-Ultrasonic NDE: Ice–Cold Ultrasonic Waves for the Detection of Damage in Complex-Shaped Engineering Components. IEEE transactions on ultrasonics, ferroelectrics, and frequency control, 65(4), pp.638-647.
[24] Taheri, H., et al.: Fast ultrasonic imaging with total focusing method (TFM) for inspection of additively manufactured polymer composite component. In: 27th ASNT Research Symposium, March 2019, pp. 212–220, 2018
[25] Raišutis, R., et al.: Application of ultrasonic guided waves for non-destructive testing of large and complex geometry engineering structures. Vibroeng. Proc. 14, 87–90 (2017)
[26] [Krautkrämer, J. and Krautkrämer, H., 2013. Ultrasonic testing of materials. Springer Science Business Media.
[27] MANUAL, T., 1988. Ultrasonic testing of materials at level 2.

DEPARTMENT OF INDUSTRIAL AND MATERIAL SCIENCE
CHALMERS UNIVERSITY OF TECHNOLOGY
Gothenburg, Sweden
www.chalmers.se

CHALMERS
UNIVERSITY OF TECHNOLOGY